POLITECNICO DI TORINO

Collegio di Ingegneria Energetica

Corso di Laurea Magistrale
in Ingegneria Energetica e Nucleare

Tesi di Laurea Magistrale

Design and formulation of materials for energy storage applications

Relatori
prof. Andrea Lanzini
prof. Adriano Sciacovelli

Candidato
Marisa Mastroleo

Marzo 2020

Table of content

Table of figures

Abstract

Driven by expanding population, growing economies and demanding quality of life, the worldwide energy consumption rates are predicted to grow unceasingly. The increasing energy consumption is expected to cause adverse impacts on the global environment due to the substantial use of fossil fuels and the consequent emission of greenhouse gases. Therefore, the effective conservation of energy represents a significant issue nowadays. The aim of this work is to present a possible exploitation of waste energy sources through suitable Form-Stable Phase Change Materials (FPCM) The manufacturing of FPCMs offers a sustainable, clean, flexible and compact option for storing thermal energy. Thanks to their large latent heat content, they are characterized by a higher energy density compared to the traditional storage solutions based on sensible energy. Furthermore, they have proven to be a more effective option for a wider range of temperature applications. In this work, the selection, mixing and compressing of a Solar Salt eutectic mixture with a supporting material and a carbon-based component allowed the thermal properties enhancement and, at the same time, the controlled sintering procedure prevented the typical leakage issues of common PCM-based solutions confirming the replicability of the whole procedure.

Summarizing, the present study contains three main contributions: the assessment of a reliable and replicable manufacturing procedure for the fabrication of FPCM pellets; an accurate investigation on the shape-stability concept in FPCMs in order to find the links between micro-structural features and thermal performances and, finally, the modelling of two possible applications of PCM for power production exploiting waste heat sources.

Scope and Motivation

Research and development in waste heat recovery and re-use have received significant attention in recent years. In 2017, around 68% of the energy consumed in the United States was wasted, without having performed any useful function, mainly in the form of low grade heat discharged to the environment.[1] This work proposes to reuse the wasted thermal energy through the pyroelectric or thermoelectric effect in order to produce the electrical energy requested by electronic devices. In fact, the lost heat can be perceived as the heat rejected by the facilities in the environment. So, the recovery and reuse of this heat offers the possibility of reducing energy costs. Pyroelectric materials are capable of converting time-dependent temperature and/or stress directly into electrical energy. In the limiting case, the PE can be placed in thermal contact with the hot and cold sources. Then, heat is transferred by conduction. This presents the advantage of being inexpensive and easy to implement. However, the thermal response of the PE heated by heat conduction is expected to be slower than that obtained with other heat transfer modes. Indeed, conductive heat transfer is a diffusive process limited by thermal contact resistance between the PE and the cold or hot plates. One of the significant challenges with the pyroelectric technique is to efficiently generate rapidly time varying temperature gradients across the device from waste energy streams that possess constant or very slow time varying temperature gradient. In the case of a temperature profile with a step variation there is the possibility to couple the pyroelectric material with a Phase Change Material to take advantage of the thermal capacitance of the material able to still have a time temperature evolution even if the temperature source is constant. Ferroelectric materials require temporal fluctuation of temperature, whereas thermoelectric devices profit from temperature spatial gradients thus leading to different applications targets. Ferroelectric materials may harvest perfectly the available thermal energy whatever the materials properties (limited by Carnot conversion efficiency) whereas thermoelectric material's efficiency is limited by materials properties (ZT figure of merit). One of the most promising possibilities for the use of a thermoelectric device is the matching with a PCM to take advantage of the fact that during the phase change the temperature is almost constant, thus two different PCMs at the sides of a thermoelectric material can enhance the possibility to have a spatial temperature difference.

ROADMAP

Experimental procedure

- Fabrication
- Thermal analysis
- Micro-structural analysis

Thermoelectric application

- Model and validation
- Results

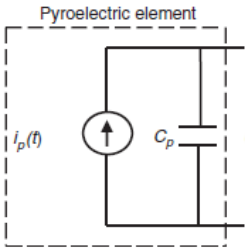

Pyroelectric application

- Model and validation
- Results

1. INTRODUCTION

The limited reserve of fossil fuels and concerns over greenhouse gas emissions make the effective utilization of energy a key issue. Therefore, the energy sector is an evolving machine influenced by many variable factors leading to an increase urge to re-shape the global energy landscape.

One of the main debated issues in the latest years has been denoted as the Energy Transition which is the structural changeover of the energy system from the current energy production and distribution system relying mainly on fossil fuels consumption to low-carbon and more efficient ones.

The main reason for the emerging figure of the TES storage technologies is strictly connected to the matching energy demand and supply of Renewable energy technologies to sustain energy supply in periods of scarce availability of the resource and to collect the surplus produced when large amount of the resource is available. Renewable has always been considered the solution for a more sustainable production and distribution of energy, but their intermittence constitutes the main limitation requiring additional integrated solutions.

In addition, the necessity to provide a safe energy supply also in areas where the transmission and distribution of electricity for instance are problematic, have also raised the demand for the integration of such kind of technologies allowing to provide robustness to those systems.

Thermal energy can be stored as latent heat, sensible heat and thermochemical heat. Among these, latent heat storage by using phase change materials (PCMs) is a promising method due to high amount of absorb and release latent heat during a phase change process between solid-solid or solid-liquid phase over a narrow temperature range.
PCMs have been applied in various applications such as energy efficient building materials and solar energy storage. However, leakage of PCMs during solid-liquid phase change process limits its application. To overcome this problem, many researchers have opted to prepare form-stable composite PCMs by compounding PCMs with porous materials.

Using PCM for TES provides a solution to increase the efficiency of the storage. PCM exhibits a high enthalpy of fusion with the ability, in a relatively small volume, to store or release large amounts of energy as latent heat during melting and solidification.

1.1 Thermal Energy Storage (TES)

Thermal energy storage can have a dual function: in the case of conventional energy sources, it can be used as a make up for temporary drops in production in order to guarantee the expected level of demand; in case of renewable energy production, added value is made by making this production quantitatively predictable.

The available technologies are various with different performance characteristics, times and response methods to demand variations.

The storage of thermal energy is favorable in all cases where energy is available directly and will be used in the form of heat; avoiding transformations from a form of energy to the other, indeed, unnecessary losses are eliminated, in accordance with the second principle of thermodynamics.

The most important characteristics of a storage system are the duration, or the time in which the energy can be conserved with acceptable losses and volume, that is, the energy accumulated per unit of volume: an efficient storage should have long life and low volume; we also need to minimize thermal losses and allow a high recovery of energy during the extraction.

Efficiency of a thermal storage system can be defined as the ratio between the energy extracted and the stored energy:

$$\eta = \frac{m_c(T - T_0)}{m_c(T_{inf} - T_0)}$$

where mc is the total heat capacity and T_{inf} is the maximum temperature at the end of the loading process.

There are three main methods of heat storage: sensible heat (heating of a material), latent heat (melting and solidifying, vaporization and liquefaction) and thermochemical energy (bond energy). The complete process involves three phases: loading, storage, unloading.

For what concern the choice of available materials, there is a great variety depending on the characteristics and the temperature range of the system. In general, materials that exhibit a large variation in internal energy per unit of volume minimize the space required; however, there are other factors to consider, such as vapor pressure, toxicity, corrosiveness, as they are very influential on the cost of the casing and therefore on the overall cost of the system.

The benefits of using TES can relate to:

-increased energy production capacity: energy may be needed in periods of low demand and stored for later use;

-reduction of energy consumption from fossil fuels and reduction of pollutant emissions;

- the shift of energy purchases in low-cost periods, with consequent reduction of operating costs;

-integration with other functions;

TES methods are classified as sensible heat thermal energy storage or latent heat thermal energy storage.

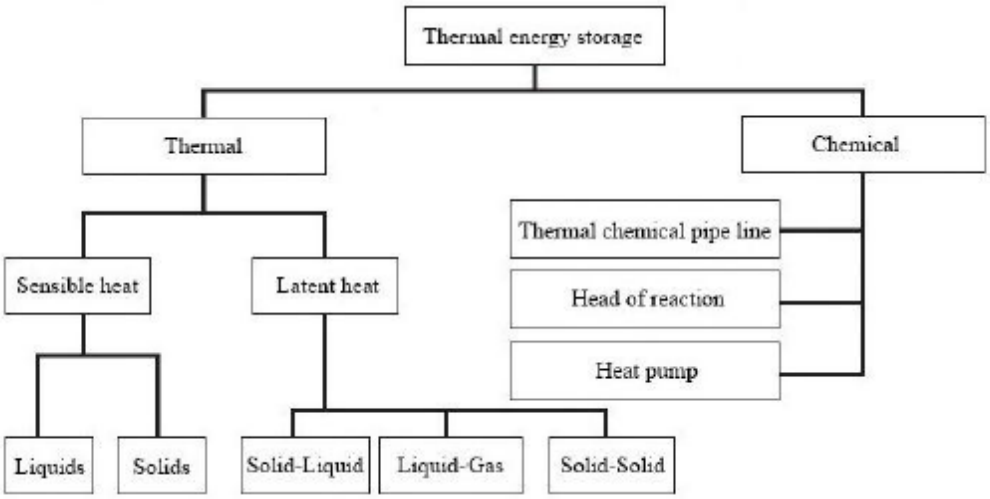

Figure 1-1-1 Types of energy storage[2]

1.1.1 SHTES

Energy is stored by changing the temperature of a liquid or solid medium without any phase change in the process temperature range.

In the case of solids, the material is in porous form and the heat is accumulated or extracted through the flow of a liquid or a gas.

A sensitive heat storage is made up of the storage material, the container and the inlet and outlet devices.

SHTES occurs when a material is driven to increase or decrease its temperature. The effectiveness of the method depends on the specific heat capacity of the material and,

if volume is an important consideration, on the material's density. The amount of heat stored is a function of the specific heat of the medium.

$$\boldsymbol{Q = \int_{T_i}^{T_f} m\, Cp\, dT}$$

Where Q is the quantity of stored heat (J), T_i and T_f are the initial and final temperature (°C), m is the mass of heat storage medium (Kg) and Cp is the specific heat (J/KgK).

The ability to store energy for a material considered depends on the cp value.

A good material must have good thermal capacity and should be cheap. Other parameters to consider in the choice are the speed of heat extraction (function of thermal diffusivity), corrosivity, operating temperature.

1.1.2 LHTES

Recent development technologies have demonstrated the possibility of accumulating large quantities of heat by taking advantage of the change in the state of the materials, without significant changes in temperature levels. The high density of energy storage (also equal to 100 KWh/m^3) and the reduced temperature variation make this a very promising type of thermal storage.
These materials can be used in the building industry, by storing solar thermal energy during the day and use it to heat rooms afterwards, without requiring other transport energy.
Latent heat storage can be classified, based on the phase change process used, as solid-solid, solid-liquid, solid-gas and liquid-gas.
Solid-gas and liquid-gas transformations are not usually utilized, despite the high latent heat, as the significant volume changes make the system complex and expensive. For this reason, the attention of the researchers has focused on the solid-liquid and solid-solid transitions, which have a high energy density per unit volume.

The heat associated with solid-solid transformations (in the passage from one crystalline form to another) is low, therefore the most common choice regards the transitions solid-liquid, thanks to the high accumulation density and the reduced volume changes required.

Initial trials took advantage of the phase change of inorganic materials, especially hydrate salts, non-flammable and inexpensive. Even today many practical systems use solutions of salts in water, even tough have many disadvantages, such as corrosiveness, instability, improper re-solidification, tendency to overcool, instead of crystallization with heat release.

For this reason, subsequent research has focused on the use of organic materials, which however present other problems such as high costs, flammability and toxicity of the fumes, substantial variations in volume.

During a phase change, thermal energy is used to break molecular bonds and allow the passage of state (fusion or vaporization) without temperature variation. Being an endothermic process, it accumulates heat, making it available later. The stored energy (E) is a function of the mass and of the latent heat of fusion.
Latent heat storage relies on the material's phase change enthalpy to store heat within a narrow temperature range, providing greater energy density [kWhth/m^3] than that achievable with sensible heat storage over the same temperature gradient; however, volumetric expansions during the melting process can reach 10 to 15% for some materials.
Phase change thermal energy storage system offer a number of advantages over the systems such as the small temperature difference between the storage and retrieval cycles, small unit sizes and low weight per unit storage capacity.[3]

The storage capacity of a LHS system with a PCM is given by:[4]

$$Q = \int_{T_I}^{T_m} m\ Cp\ dT + m a_m \Delta H_m + \int_{T_m}^{T_f} m\ Cp\ dT$$

Where a_m is the fraction melted and ΔH_m is the heat of melting per unit mass (J/Kg).

Latent heat has the main feature of having considerably higher values compared to sensible fractions for usual temperature changes. As a consequence, storage systems applying PCMs are able to store a larger amount of heat in the same volumes and operating temperature ranges. Equations show that contributions to the latent heat are the two sensible fractions operating the sensible temperature increase and the latent fraction stored/released at nearly constant melting temperature Tm.

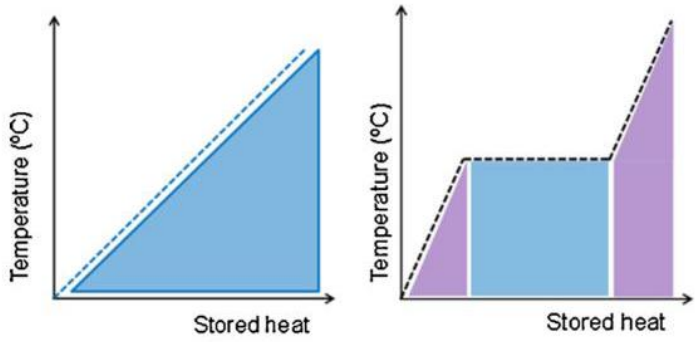

Figure 1-2 Thermal energy storage principles[5]

It is clearly impossible to choose the perfect storage material with the best performance, the selection must be a an optimum amongst all the thermo-physical properties and performance of the materials, especially for a given admissible temperature range of the material before the latter degrades.

The spread of the use of phase change materials depends on the development of effective containment methods. The issues linked to the phase change and the nature of the substances used, they require the use of more expensive materials than those of containers for water or rocks.

The main characteristics required of a containment material are: mechanical strength, flexibility, corrosion resistance, structural and thermal stability and easy management.

Containment must act as a barrier between the PCM and the surrounding environment (capable of preventing loss of material, entry or exit of water, oxygen penetration and consequent oxidation.) and must provide a sufficient area for heat exchange, with good heat conduction characteristics.

Among the various possibilities there is also the encapsulation of the PCM.

The ideal PCM should meet several criteria related to the desired thermophysical, kinetic and chemical properties. In addition to the melting characteristic in the required temperature range, the properties to be taken into account when choosing a material are thermodynamic but also kinetic, chemical, technical and economic.

They are listed below.

Thermal properties:

- A melting temperature in the desired operating range,
- A high phase transition latent heat per unit volume,
- A high specific heat, to provide significant additional SHS,
- High thermal conductivity of both phases.

Physical properties:

- A small volume change on phase transformation,
- A low vapor pressure at the operating temperature,
- Favorable melting of the PCM,
- Congruent melting of the PCM,
- A high density.

Kinetic properties:

- No super cooling,
- A high nucleation rate,
- An adequate rate of crystallization.

Chemical properties:

- Long-term chemical stability,
- A completely reversible freeze/melt cycle,
- Compatibility with the construction materials,
- No corrosion influence on the construction materials,
- Non-toxic, non-flammable, non-explosive to ensure safety.

Typical PCM disadvantages include:

- Super-cooling. Majority PCM do not solidify immediately once the temperature is lower than the phase change equilibrium temperature.
- Phase separation.
- Low thermal conductivity. For example, thermal conductivities of most organic PCMs are less than 0.4 W/mK.

One of the main properties of commonly used PCMs is their low thermal conductivity, usually between 0.2 and 0.7 [W/mK], requiring the use of complex heat exchanger geometries to obtain required heat transfer rates from latent heat storage containers. Conventional techniques to overcome the low heat transfer characteristic rates would be the used of metal fins ; however novel promising techniques such as carbon cloths , shape stabilized PCMs with graphite, microencapsulated-PCM slurries and direct contact latent heat storage systems, can also be used to increase the global UA value of latent heat storage systems.

Despite the studies already carried out, some issues remain to be explored:

-solidification: many materials are not suitable for the purpose because they exhibit irregular behavior during crystallization; others crystallize too slowly or are not stable;

- overcooling: during the freezing of the material the temperature drops below the melting point before that solidification begins. Hydrated salts have a significant tendency to overcooling: the rate of nucleation (of the crystals from the fluid) and growth of the nuclei it is very slow, therefore the fluid is cooled, it does not solidify at the melting point. This behavior is related to the viscosity of the fluid at the melting point.

-nucleation: the problem of overcooling can be mitigated by adding additives that favor homogeneous or heterogeneous nucleation. In homogeneous nucleation, the

nucleation rate of the crystals is increased without adding foreign substances: for example ultrasound waves can be used, increasing the diffusion of ions, creating cavities that act as nucleation centers; in heterogeneous nucleation, the walls of the container or the impurities present in the fluid act as catalysts for nucleation[6] .

TES System	Capacity (kWh/t)	Power (MW)	Efficiency (%)	Storage Period	Cost (€/kWh)
Sensible (hot water)	10–50	0.001–10.0	50–90	days/months	0.1–10
Phase-change material (PCM)	50–150	0.001–1.0	75–90	hours/months	10–50
Chemical reactions	120–250	0.01–1.0	75–100	hours/days	8–100

Figure 1-3 Typical parameters of TES systems[2]

1.2 PCM Classification

Latent Heat is the amount of enthalpy which is necessary to provide or withdrawn from a system allowing a phase transition of it, substances or composite materials exploiting this source of heat, acting both as a sink and as a source in the reverse process, are the termed Phase Change Materials or PCMs. During a phase transition, a thermodynamic system absorbs and releases a fixed and constant amount of energy, similarly PCMs undergo a reversible process of storing and releasing heat when required during a certain number of cycles depending on the lifetime of the materials involved.

A considerable number of PCM is available in any desired temperature range. According to their chemical composition, PCMs can be categorized as organic compounds, inorganic compounds and eutectic mixtures. Each group has its typical range of melting temperature and its range of melting enthalpy.[7]

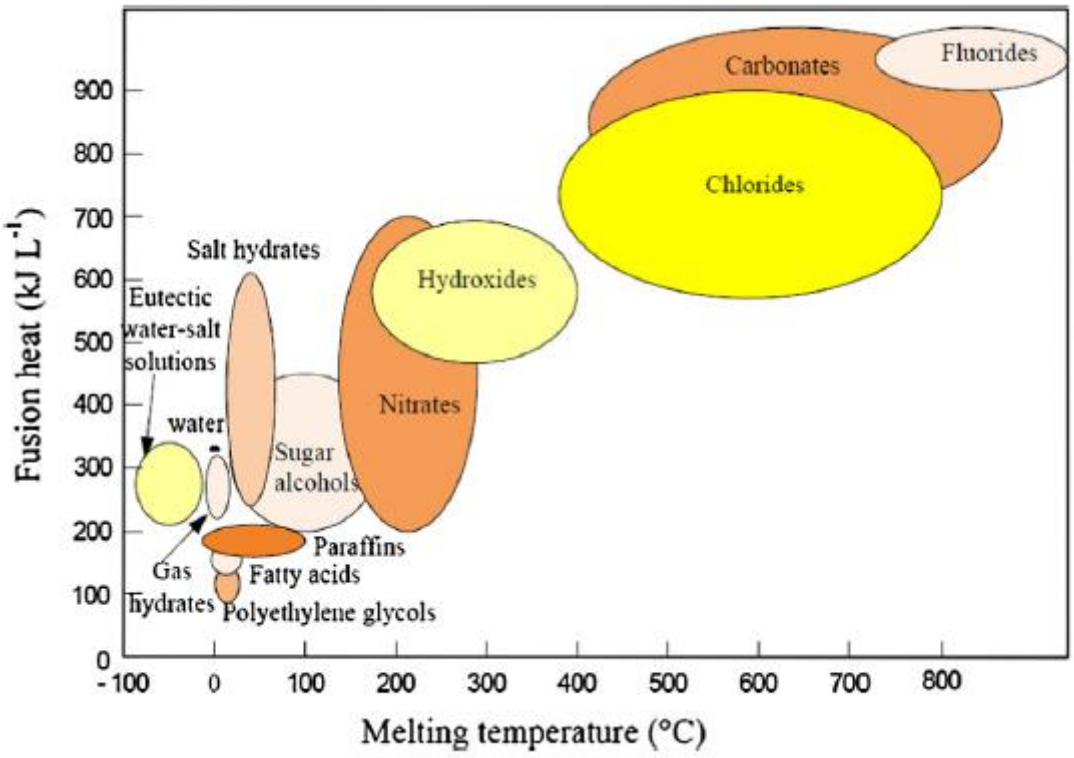

Figure 1-4 **Fusion heat and melting temperaure for some PCM**[8]

PCMs can be divided into three main groups – based on the temperature ranges over which the TES phase transition occurs: (i) low temperature PCMs – with phase transition temperatures below 15 °C, usually used in air conditioning applications and the food industry; (ii) mid temperature PCMs, the most popular – with phase transition temperatures in the range 15–120 °C with solar, medical, textile, electronic and energy-saving applications in building design; (iii) high temperature PCMs with a phase transition above 120 °C developed mainly for industrial and aerospace applications.

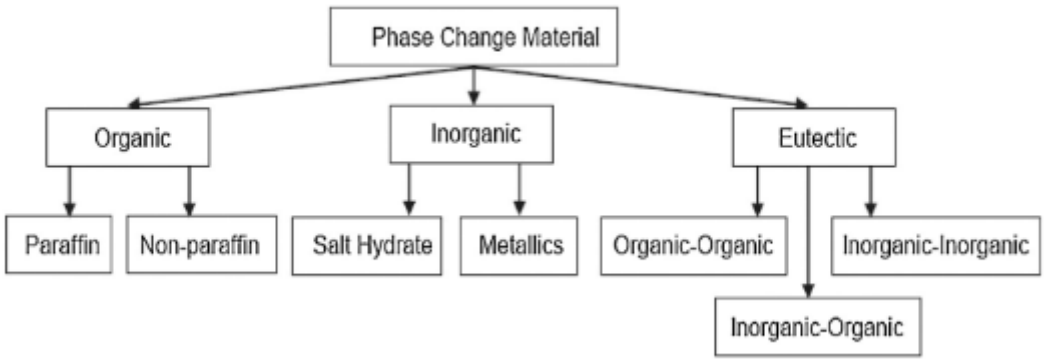

Figure 1-5 **Classification of PCM**[2]

Organic materials including paraffins and non-paraffins are the most widely used and commercialized PCMs especially for domestic applications. Paraffins materials in particular, have a melting temperature between -18 to around 30°C (in the range of human comfort temperature), non-corrosivity, non-toxicity, good chemical stability so that they are preferably used for space heating/cooling buildings applications. Because of their large availability in the market they are also cheap compared to other types of PCMs. Some specific kinds of paraffin waxes with a different or higher carbon composition allow gaining higher latent heat and melting temperatures expanding the window for the application of such materials. The same happens for fatty acids in the subcategory of the non-paraffins PCM, the latter however undergo a sharper phase change compared to others occurring at higher temperatures.

Common drawbacks of organic PCM in general include their very poor thermal conductivity but more specifically, the main limitations about using paraffins are related with flammability and non-negligible volume change (around 10%) on the other hand non-paraffins are corrosive, highly flammable and toxic. Non paraffins however do not experience phase segregation or sub cooling and are generally chemically stable. Amongst Non-paraffins, sugar alcohols present the highest melting temperatures and latent heats at lower prices but with high chemical instability which leads to more attention to be paid in the design phase.

Inorganics counting molten salts, salt hydrates and metals have generally highest melting temperatures and latent heat, one of the most important benefits is the high thermal conductivity. These materials however experience a lot of disadvantages connected mainly with the use of salt hydrates specifically. The latter show phase segregation and super cooling issues, corrosion when in contact with metal containers and high thermal instability. On the other side, metals reach the highest thermal conductivity but with low latent heat and low specific heat and, in addition to this, they are also very expensive.

Eutectics are binary or multiple mixtures of organic-organic, inorganic-inorganic or organic-inorganic materials. In general, they do not experience phase segregation issues, present good thermal conductivity and have higher melting temperatures. Even if some researchers claim that thermal properties for eutectic mixtures can be evaluated with some accuracy, salt eutectics for example have specific thermo-physical properties changing compared to the single pure salts composing them, so that they should be experimentally determined.

2. FORM-STABLE (SHAPE-STABILIZED) PCMs

As previously revealed, often in parallel with the use of a material is necessary to face the limit of heat exchange properties. One possible solution to minimize this problem is to merge the PCM into a highly conductive medium (typically a metal base); where this option is not available, it is possible to resort to all encapsulation of the substance in order to balance low conductivity with a high heat exchange surface. Also in this case the choice of the best solution depends on the physical parameters of the material combined with specific requests from the system in which you are operating.

An approach of this type is capable of providing further benefits, such as preventing chemical reactions between PCM and external substances, increase compatibility with other components of the storage system and improve its handling.

Some of the main issues related to the inclusion of the PCM materials inside devices regard leakage and chemical compatibility when in contact with other containment materials or with the flowing HTF.

This has led to finding innovative solutions including encapsulation technologies, whether macro or micro, impregnation methods inside construction materials or shape stabilized PCMs.

A shape-stabilized phase change material is composed of working substance and supporting material. The working substance stores or releases latent heat during the melting or solidifying processes, whereas the supporting material prevents the melted phase from leaking so the whole system remains in solid state.

The selection of suitable supporting materials and shape-stabilizing strategy is crucial in designing ssPCMs for practical applications.

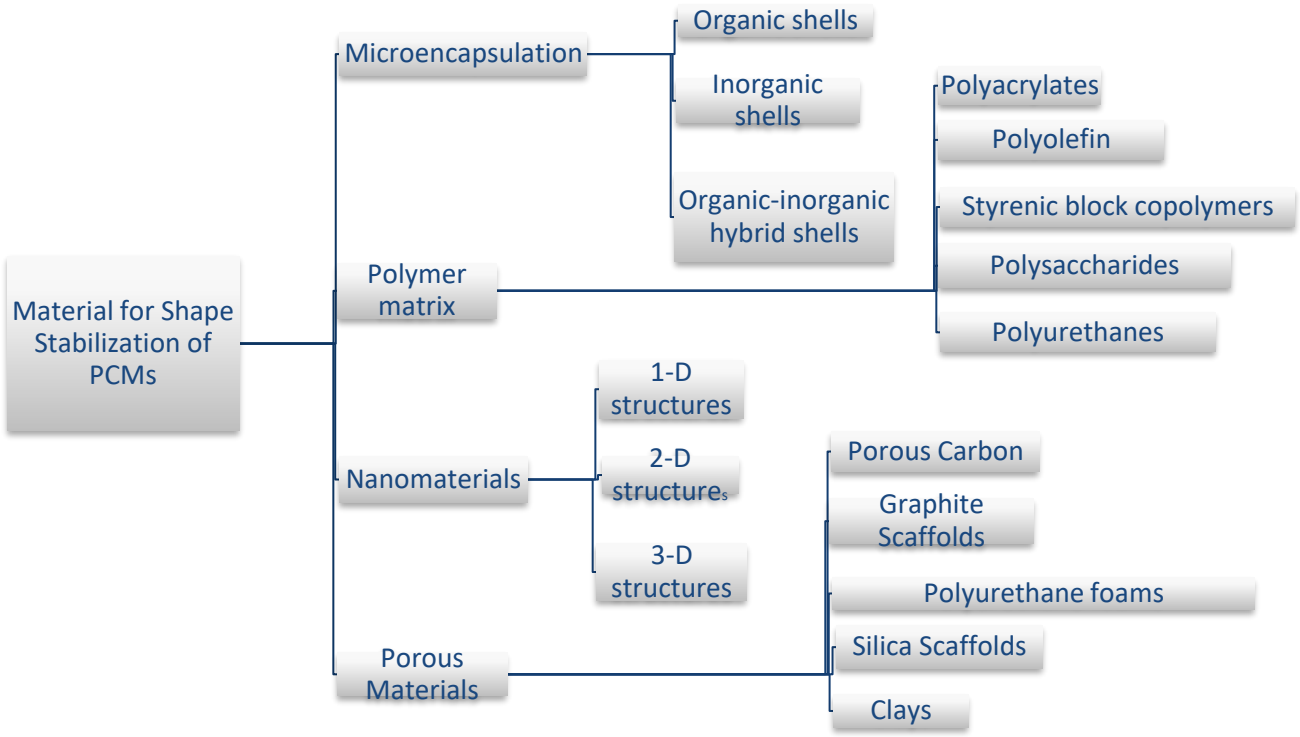

Figure 2-1 Diffrerent marials for shape stabilization

(Micro) encapsulation techniques provide opportunities to fabricate advanced PCMs with a greater heat transfer area, reduced reactivity with the outside environment and controlled volume changes during the phase transition. The microencapsulation systems mainly suffer from low heat transfer rate, high cost for microencapsulation preparation and limited application fields.

Microcapsules can be described as particles that contain core material surrounded by a coating or shell and have diameters in the 1-1000µm range. Microencapsulation is widely used in commercial applications including carbonless copying paper, functional textiles, adhesives, cosmetics, pharmaceuticals and other medical applications.[9]

Microencapsulation is carried out via three techniques called physical methods, chemical methods and physic-chemical methods.[10] The physical methods contain techniques such as spray cooling, sprays drying and fluidized bed processes and the chemical methods contain in situ polymerization and solvent extraction/evaporation method. The physic-chemical methods contain simple and complex Coacervation as well as sol gel technology.

When the costs of encapsulation and those related to the increase of PCM conductivity are analyzed, the increasing attention being given to the development of composite

materials, is clearly the rational approach, using inorganic or organic supporting materials.

Porous materials with attractively high surface areas, high pore volume, ready mass transport properties and high storage capacities, have been widely used in various applications such as adsorption, catalysis, energy conversion and storage, etc. Integrating porous supports and PCMs armed the ss-PCMs with enhanced durability performance, thermal conductivity, thermal stability and chemical stability by choosing or constructing the desirable porous supports. Especially, pore confinement and the mutual interaction between pore surface and PCMs molecules can profoundly affect the physical properties of fluids and avoid the leakage of PCMs during the phase change process.

	Macro-encapsulated PCM	**Micro-encapsulated PCM**	**Form-stable PCM**
Status	Mature level	Further research needed on some techniques against leakage issues	Ongoing research
Development sector	Industrial/domestic sectors	Lab research, Industrial sector	Lab research, prototype level
Cost	High cot	Wide range of prices depending on the technique adopted	Low cost
Supercooling	Yes	No	Not demonstrated
Phase separation	Yes	Only for salt-Hydrated PCMs	No
Deformation	Yes (in the long term and for some types only)	No	Controllable volume variations
Leakage	Yes (in the long term and for some types only)	Yes, at micro-scale	Yes, depending on the manufacturing
Agglomeration	No	Yes	Possible
Heat transfer enhancement	Higher only with metal shells or finned-metal/conductive plates	High (further enhanced when combined with nanofluids)	High (further enhanced when combined with carbon-based nanostructures)

Table 2-1 Comparison between different ways to shape stabilize PCMs

The most commonly used methods for producing SSPCMs are:

- Vacuum impregnation
- Mixing and cold compression
- Hot compression
- Direct impregnation
- Mixing and stirring of mixtures

2.1 Mid-Low Temperature ssPCMs

PCM find application in the building industry, textiles the automotive sector and solar energy installations. Depending on the application there is the need to find a composite PCM in the proper temperature range.

2.1.1 Organic Supporting Materials

Polyethylene (PE), due to its properties and chemical affinity to paraffins, is widely used in form-stable PCMs as a supporting material. Sari[11] prepared paraffin/HDPE composites as SS-PCMs by melt mixing. The maximum amount for two different types of paraffin in the PCM composites were 77% and it was observed that the paraffin was well dispersed in the solid HDPE matrix. In addition, to improve the thermal conductivity of the SS-PCMs, graphite, expanded and exfoliated by heat treatment, was added and increased the thermal conductivity by 14‑24%.

Umair et al[10] used two paraffins with melting temperatures of 48-50°C (P1) and 63-65°C (P2) to prepare the composites with HDPE. The leakage test showed that the mass fractions of paraffins in the composites could go high as 76% without any leakage of the paraffin. The thermal conductivity of the composite improved about 33% for the P1/HDPE and 52.3% for P2/HDPE when 3% of expanded and exfoliated graphite was introduced.

The structure of poly(vinyl chloride) (PVC) gives rise to a relatively tough and rigid material able to accept a wide range of additives, including PCMs. In this context, blends of PVC/PA and PVA/PA were investigated by Sari et al[12]. They established that there was no leakage of PA even in the molten state and that the maximum miscibility ratio of PA with both polymers was found at the level of 50% while maintaining the shape-stabilization effect.

The use of fatty acids such as stearic acid (SA), palmitic acid (PA), myristic acid (MA), and lauric acid (LA) as shape-stabilized PCMs increases their feasibilities in practical latent heat storage applications. A series of fatty acid/poly (methyl methacrylate) (PMMA) blends, such as SA/PMMA, PA/PMMA, MA/PMMA, and LA/PMMA were prepared by Fang et al[13] as new kinds of ssPCMs by encapsulating fatty acids into PMMA which acted

as supporting material. The shape-stabilized fatty acid/PMMA blends have high latent heat storage capacity and proper phase change temperatures at range of 40–70°C. However low conductivity is the major drawback associated with the fatty acid due to which there were various kinds of materials tested with these fatty acids; these materials includes finned configuration [14], dispersion of high conductivity particles, addition of metals or using porous structure material with high thermal conductivity.

Peng et al[15] used styrene-b-(ethylene-co-butylene)-b-styrene triblock copolymer (SEBS) as a supporting material to prepare SEBS/paraffin ssPCMs. In this study the composite latent heat is of 189 J/g, the 75% of the latent heat of the pure paraffin.

Unlike other polymer matrices, polyurethane matrix is a latent heat storage material as it can undergo solid-solid phase transition. In addition, it can act as a supporting material to load other organic PCMs. This approach not only just removes the leakage problem but also allows the formation of high thermal energy storage density PCM composites.[16]

2.1.2 Inorganic Supporting Materials

Different methods have been reported to fabricate carbon material composite PCMs. The simplest method is simply mixing the powder-like solid PCM with carbon powder/nanomaterials to form powder mixture. The formed powder mixture could also be compressed into the designed shape at the ambient temperature, which was known as cold compression.

Paraffin (n-docosane)/expanded graphite (EG) composites prepared by absorbing liquid paraffin into the EG, as a form‑stable PCM were studied by Sari et al.[11] Because of the capillary and surface tension forces of EG no leakage of liquid paraffin was observed during the phase transition. Fatty acid/expanded graphite (EG) composites prepared by a vacuum impregnation method were investigated, too. It was found that the maximum fatty acid absorption of EG was 80 wt% without molten fatty acid oozing from the composites.

Wang et al [17] investigated the composite made by blending PEG with expandable graphite. The maximum mass percentage of PEG dispersed in PCM composites without any leaking of the polymer was found to be as high as 90 wt.%. It is of interest that the thermal conductivity was considerably increased because of the thermally conductive network formed by the EG's porous structure. One issue of the EG is related to phase separation.

Most clay mineral materials have porous structure with high specific surface area. Thus, clay mineral materials can effectively load PCMs by various interactions, such as capillary force, surface tension, hydrogen bond, Van der Waals' force. The common porous clay mineral materials include expanded perlite, diatomite, sepiolite, attapulgite,

vermiculite, fly ash, etc. due to their high thermal stability, chemical compatibility, thermal reliability and moderate price.

The capric acid (CA) – myristic acid (MA) eutectic mixture/vermiculite (VMT) composites were prepared as a shape- stabilized PCMs using vacuum impregnation method. The CA–MA eutectic mixture could be retained by 20 wt% into pores of the VMT without melted PCMs seepage from the composite. The thermal conductivity of the shape-stabilized CA–MA/VMT composite PCMs is increased by about 85% by adding 2wt% expanded graphite (EG) into the composite. The melting temperature is 19.75°C.

The thermal conductivity of porous clay minerals based PCMs is quite low, compared with other carriers such as EG. It is reported that the heat transfer rate would be enhanced via incorporating additional additive to expanded perlite/PCMs matrixes. For example, Zhang et al[18] coated expanded perlite with carbon layer (EPC) via in situ carbonation as support to increase the thermal conductivity of PEG/EPC. As a result, PEG/EPC ss-PCMs composite with 66.38 wt % PEG exhibited good thermal reliability after 200 melting/freezing cycles, high thermal conductivity with 0.479W/mK, and good chemical stability.

An investigation on a new type of shape-stabilized phase change material (PCM) prepared by impregnating eutectic salt hydrate (Na2SO4·10H2O-Na2CO3·10H2O with 1:1 in mass ratio) into expanded vermiculite (EV) is carried out by Xie et al[19]. The maximum mass percentage of Na2SO4·10H2O-Na2CO3·10H2O eutectic within the composite is determined as 60%. The phase change temperature and the melting enthalpy of the composites are 23.98 °C and 110.3 J/g respectively. The thermal conductivity is of about 0.192 W/mK.

A novel form-stable LiNO3‑NaNO3‑KNO3‑Ca (NO3)2/calcium silicate composite PCM was developed by cold compression and sintering. The eutectic quaternary nitrate is used as PCM, while calcium silicate is used as structural supporting material.[20] This composite PCM has a low melting point (103.5°C) and remain stable without decomposition until 585.5°C. Thermal conductivity was measured to be 1.177 W/mK and that could be added using thermal conductivity enhancers.

Carbon fibers are resistant to corrosion and chemical decomposition and are compatible with most PCMs. Carbon fiber has a thermal conductivity similar to those of aluminum and copper and the density of carbon fiber is theoretically less than 2260 kg/m3 which is lower than that of the meals that are usually used to enhance conductivity. However, there are a number of issues, including limited loadings and therefore limited enhancements, poor homogeneity and stability. Jiang et al[21]prepared a novel composite PCM with paraffin and carbon fiber. The CBCF monolith was prepared following a slurry molding method. The interconnected open structure within the CBCF network, allow the

molten paraffin to be held inside the matrix due to capillarity forces and surface tension. Increasing carbon fiber density from 0.09 g/cm3 to 0.39 g/cm3 the thermal conductivity increases from 4.37 W/mK to 13.82 W/mK but the anisotropic differences increase.

The shape-stabilized paraffin /silicon dioxide (SiO2) / expanded graphite (EG) composite PCM was prepared by the sol–gel method. Silica gel acted as the supporting material and EG was used to increase the thermal conductivity. The mass fractions of the SiO2 and EG were 20.8% and 7.2%, respectively. The phase-change temperatures of the paraffin / SiO2 composite and the paraffin /SiO2 /EG composite are 27.53 °C and 27.72 °C, respectively. The test results indicated that thermal conductivity of theSiO2/paraffin composite and the SiO2/paraffin/EG composite are 28.2% and 94.7% higher than that of paraffin (0.1264W/mK),respectively.[22]

As a continuous skeleton structure, metal foams with high strength-to-density ratio, high open porosity, large pore size (0.1-5mm), and relatively high thermal conductivity, are believed to be promising supports for improving the overall thermal conductivity. Xiao et al[23]used copper and nickel foams, both with 95% porosity and 1-5mm pore sizes, to fabricate composite PCMs with paraffin. The effective thermal conductivity was increased from 0.305 W/(m K) of pure paraffin to 4.9 W/(m K) of paraffin/copper foam composite PCM, and to 0.95–1.3 W/(m K) of paraffin/nickel foam composite PCM. Meanwhile, the phase change temperature was maintained at almost the same point, but the specific heat and latent heat were reduced by 14–24% and 22–30% because of the low specific heat and non-phase change of the metal skeleton, respectively. Furthermore, the authors pointed out that the effective thermal conductivity of composite PCM decreased with the increase of porosity and hardly affected by pore size.

Two different procedures can be adopted for impregnating PCM into the porous foam. Warzoah et al[24] compared simple submersion infiltration and vacuum impregnation using paraffin and carbon foam. The results revealed that with simple submersion the impregnation ratio was about 75%, while the vacuum impregnation was much more effective with almost 100% impregnation ratio.

2.2 High Temperature ssPCMs

Molten salts are among the most promising phase change materials for thermal energy storage at medium-high temperature. Their applications are limited due to chemical compatibility such as corrosion of containers and low thermal conductivity. The usage of ssPCMs enables to overcome these issues.

To increase he thermal conductivity, one of the possibilities is to disperse carbon allotrope into the molten salts and then compress, or to infiltrate molten salts in a prefabricated block of carbon. Although the latter possibility does not lead to phase separation (despite of the former), the resulting composites are often unable to retain enough PCMs within their structure. The use of graphite particles has many advantages such as low density in contrast to metals and high resistance to corrosion.

Relatively poor wetting between carbon materials and molten salts is an important reason for the leakage and phase separation. The poor wettability could lead to a relatively loose, porous structure.

One example of composite PCM was prepared by Ge at al[25]. It was composed by a molten salt-based PCM (LiNaCO3), a ceramic skeleton (MgO) and a carbon-based thermal conductivity enhancer (graphite flakes and carbon nanotubes). The mixture was shaped into disk-like green pellets by uniaxial compression and then sintered in an electric furnace. CNTs are much better dispersed in the salt in the presence of MgO, this is also due to the interfacial energies between the different components of the composite materials. Thermal conductivity over 5 W/(m K) can be achieved with a carbon loading of 20%. A 10% carbon loading gives a composite with a thermal conductivity over 4.3 W/(m K) and an energy storage density over 530 kJ/kg.

Lachheb et al[26] prepared a new salt LiNO3/graphite composites by uni-axial compression method. No chemical interaction between salt and graphite was detected. The thermal conductivity increased from 70% to 264% with 5% to 20% of graphite mass fraction respectively. As in the case of thermal conductivity, a linear increase in the composite thermal diffusivity was noticed with the increase of graphite mass fraction.

The main drawback is linked to the hydrophilicity of salts making them more difficult to be absorbed into EG. An eutectic salt (MgCl2-KCl) was used as a PCM in a composite with EG by Liu et al[27] with a melting point of 424.14°C. Compared with the eutectic salt, the composite PCM exhibits a reduction in supercooling and an enhancement in thermal conductivity by 11 fold. It is found that the block fabricated has a good uniformity and small volume expansion.

Metallic materials are a kind of PCM for high temperature thermal energy storage which deserves more attention. Compared with molten salts, most metallic materials have

higher thermal conductivity and larger latent heat during liquid-solid phase change. Xu et al[28] proposed a ssPCM based on Al/Al_2O_3 for a temperature range higher than 650°C; this kind of form-stable PCM can provide a solution to the corrosion issue, to the leakage and to the need of high temperature thermal storage for CSP. Al/Al_2O_3 was prepared by mixed sintering method, the samples were prepared with different molding pressure and different molding time. Longer molding time yields some leakage. Thermal analysis showed that thermal conductivity increased with increase of molding pressure possibly due to compactness and enhanced contact between each particle.

A high temperature phase change thermal storage material, composed of sodium sulphate as a phase change material (Na2SO4) and diatomite as a supported matrix, was synthesized by sintering over the melting point of the sodium sulphate.[29] Diatomite is a kind of mineral with high specific surface area, great absorbability, thermo stability and corrosion resistance capability, and it has been used as a favorable thermal storage backing material.

One of the most promising supporting materials is Vermiculite which advantageous also for high temperature application since has a relatively high melting temperature. Sodium nitrate/Expanded Vermiculite composite PCM were prepared by direct impregnation method by Li et al.[30] The melting temperature of the composite was of about 300°C. One of the main issues is related to the low thermal conductivity of EV; to solve this drawback, silicon carbide is introduced in the composite. Silicon carbide has many superior properties, such as high hardness, strength, excellent resistance to oxidation and corrosion, low coefficient of thermal expansion, and good heat-transfer capabilities. The thermal conductivities of composite were 0.70 W/(m K) at 25 °C and 0.78 W/(m K) at 300 °C, respectively.

A SSPCM review has been presented highlighting the thermal diffusivities achieved in literature.

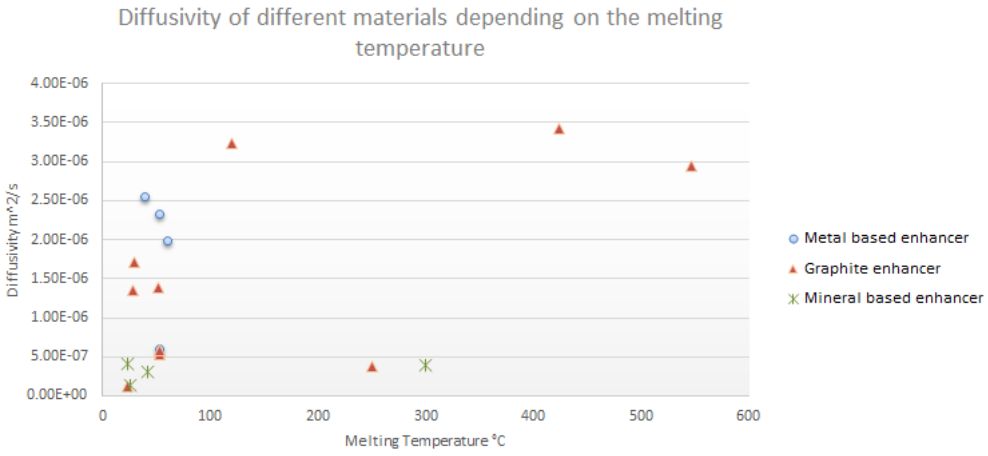

Figure 2-2 Thermal diffusivities of different PCM function of Melting temperature and thermal enhancer

3. EXPERIMENTAL PART

3.1 Materials selection and characterization

Criteria for the selection of the components range from chemical, thermo-physical to economic specifications.

The main requirement for the choice of the FPCM is the high energy density reached in a medium-high temperature range. The Solar Salt which has been selected as PCM is a eutectic of NaNO3 and KNO3, supported by Vermiculite host material and Graphite as thermal performance enhancer. One of the main criteria for the selection of such formulation is connected to chemical compatibility, all the components show no chemical decomposition in this temperature range (25-300°C) and they do not cause fire or explosion hazard and they are non-toxic, so that they can be easily handled and applied for a wide variety of applications.

The adoption of Vermiculite, as many other clays/phyllosilicates, is the main contributor to the overall shape-stability of the components.[30] [31] [19] [32] The main reason for selecting this kind of supporting material is connected to his high free surface area and absorbability, in the specific case of salts it has good interfacial energy so that Vermiculite is prone to be wetted by the Solar Salt. One drawback is connected with low thermal conductivity. In order to solve this, graphite has been selected to take part to the shape-stabilized porous structure as a thermal conductivity enhancer. Compared to many other studies adopting graphite in his more porous expanded form or in foam-like structure[33] [34] [35] [21] , in this case-study graphite has been dispersed and mixed with the other components to form the overall structured matrix.

Lastly, the main driver for the investigation of such formulation is the cost effectiveness of the materials involved. They are widely available in the market and the low cost for the fabrication process make them suitable for large-scale applications.

3.2 Fabrication process

The eutectic mixture of Potassium Nitrate KNO3 (purity > 98%) and Sodium Nitrate NaNO3 (purity >98%) in 40:60 wt% has been considered as the PCM material. The Vermiculite has been adopted as supporting material (SM) and graphite (Cg) (particle sizes 95% < 53μm) have been added in different mass contents to track thermal performance enhancement.

Following tables show the composition of Vermiculite and Graphite adopted for the formulations.

Composition	SiO2 %	MgO%	Al2O3%	Fe2O3%	K2O%	CaO%	TiO2%
Vermiculite	46.0	27.5	9.8	9.0	2.8	2.5	1

Table 3-1 **Vermiculite composition**

Composition	C%	S%	N%	Ash%	Volatile%	Moisture%
Graphite	98.6	0.05	0.05	0.8	0.3	0.3

Table 3-2 **Graphite composition**

The fabrication procedure adopted consists into three different steps: Mixing, Tableting and Controlled heating. The first experimental outcomes have been those resulting from the sintering stage is a Leakage test.

3.2.1 Mixing and Tableting

The first stage consists in a mixing procedure of the components of the formulations initially in powder form. The samples have been fabricated with and without graphite and with different Vermiculite particles size. Particle sizes of KNO3 and NaNO3 and Graphite are in the range ~µm - ~nm. All the materials used to produce the final tablets have been purchased from suppliers in the market for industrial applications.

The tableting of the 50mm diameter and 75 g weight pellets has undergone through uni-axial cold-compression conducted by means of compressing machine at 20 MPa with a preload of 5.6 N held for 1 minute.

Every step of the manufacturing process may impact in an enormous way when dealing with SSPCM, parameters like compressing pressures, increase/decrease of the components, particle sizes and the nature of the subsequent sintering process may totally change the outcomes of the Leakage tests leading to the loss of PCM from the holding matrix thus not guaranteeing the stability of the tablet.

Additional complications might arise if dealing with non-thermally and non-chemically stable composite materials causing uncontrollable and unpredictable behavior towards shape-stability at higher temperatures. In this case, all the materials involved are thermally stable in their operating range and chemically inert amongst them even at higher temperatures under their degradation temperatures.

3.2.2 Sintering and Controlled cooling

The compressed tablets have been placed into glass plates and covered on top to avoid direct radiation effects and non-homogeneous sintering.

The sintering process has been conducted in a furnace by setting a default heating program:

- Heating from 25 °C to 220°C with a 10°C/min heating rate;
- Isothermal step at 220°C for 10 min;
- Heating from 220-300 °C with a 5°C/min heating rate;
- Isothermal step at 300°C for 1 hour;
- Controlled slow cooling down of the pellets inside the furnace.

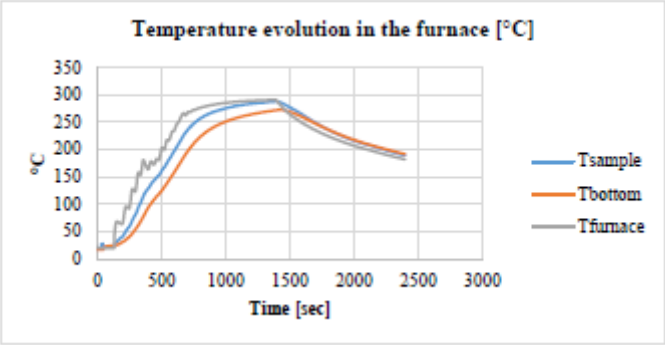

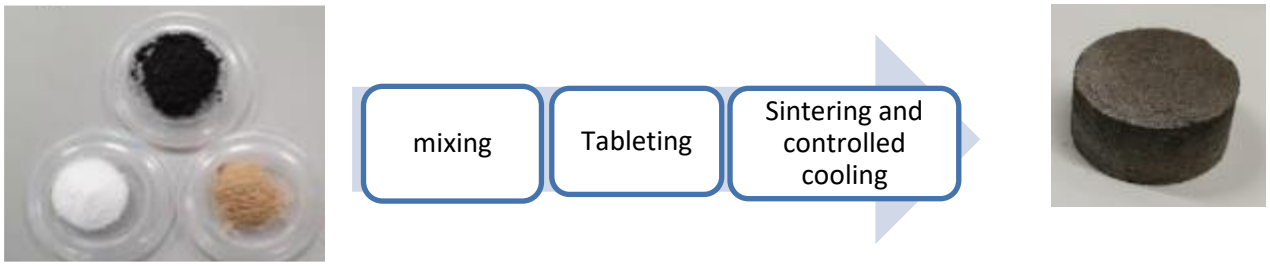

Figure 3-1 **From row materials to the composite PCM**

The starting step is higher than the second one to win the starting inertia and to speed up the heating of the furnace. The choice of the target temperatures is connected to the melting point of the PCM inside the SSPCM, in the following steps temperature has been pushed over the PCM's melting point and held for an interval of time in order to complete the sintering process of the pellets and afterwards to test the leakage of all the samples.

The sintering process plays a fundamental role in the formation of the microstructures in the composite. According to Zhiwei et al. after the compression of the pellets, the sintered composite is the result of contemporary and competing processes of rearrangement along with densification and swelling due to the presence of ceramics and carbon-based materials respectively. [35]

These processes may occur at different rates according to starting dimension, orientation, non-uniform distribution and impurities of the particles involved and most of all to the compressing conditions considered. Sintering as well as sample heating and cooling at subsequent cycles, result in differences in the porosity, free surface area, actual density and volume but also in shape and in the components distribution and morphology.

Formulation	Solar Salt wt %	Vermiculite size and wt%	Graphite wt%	Leaking Test
S5V3G0	50%	3mm 50%	0%	Yes (minor)
S5V1G0	50%	1mm 50%	0%	Yes (minor)
S5V0.25G0	50%	0.25mm 50%	0%	No
S5V3G10	50%	3mm 40%	10%	Yes(minor)
S5V1G10	50%	1mm 40%	10%	Yes (minor)
S5V0.25G10	50%	0.25mm 40%	10%	No
S7V3G0	70%	3mm 30%	0%	yes
S7V1G0	70%	1mm 30%	0%	Yes
S7V0.25G0	70%	0.25mm 30%	0%	Yes
S7V3G10	70%	3mm 20%	10%	No
S7V1G10	70%	1mm 20%	10%	Yes (minor)
S7V0.25G10	70%	0.25mm 20%	10%	Yes

Table 3-3 **ssPCMs composition**

From this preliminary test, staring hints suggest that sample with lower content of Solar Salt is likely to support and sustain PCM inside the host matrix. The increasing content of graphite is not only useful for the enhancement of the thermal conductivity but foster the overall supporting capacity of the matrix.

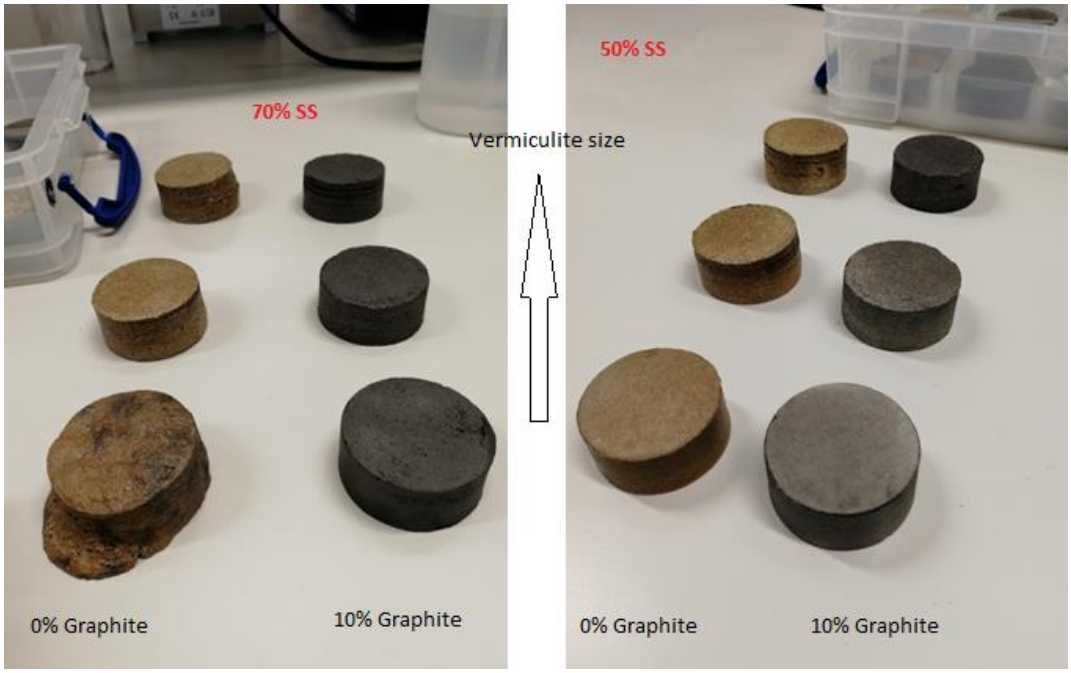

Figure 3-2 ssPCMs fabricated

The sintering process pays fundamental role in the formation of microstructures in the composite. According to Zhiwei et al.[35] after the compression of the pellets, the sintered composite is the result of contemporary and competing process of rearrangement along with densification and swelling due to the presence of ceramics and carbon-based materials respectively.

These processes may occur at different rates according to starting dimension, orientation, non-uniform distribution and impurities of the particles involved and most of all to the compressing conditions considered. Sintering as well as sample heating and cooling at subsequent cycles, result in differences in the porosity, free surface area, actual density and volume but also in shape and in the components distribution and morphology.

This may suggest that, sintering and subsequent cooling down at room temperature occurring before re-cycling (at lower temperatures) may create a definitive and reinforced final internal matrix with respect to other fabrication processes.

The final rearranged structure is an internal re-distribution of the elements constituting the formulation with a preferential organization of carbon-particles on the outer surface of the molten salt because of their poor wettability and a densification of the salt-supporting material structure. This is due to the ceramics' high wettability, thus high surface energies which keep the salt trapped inside providing local rigidity to the structure in a final reinforced overall structure.

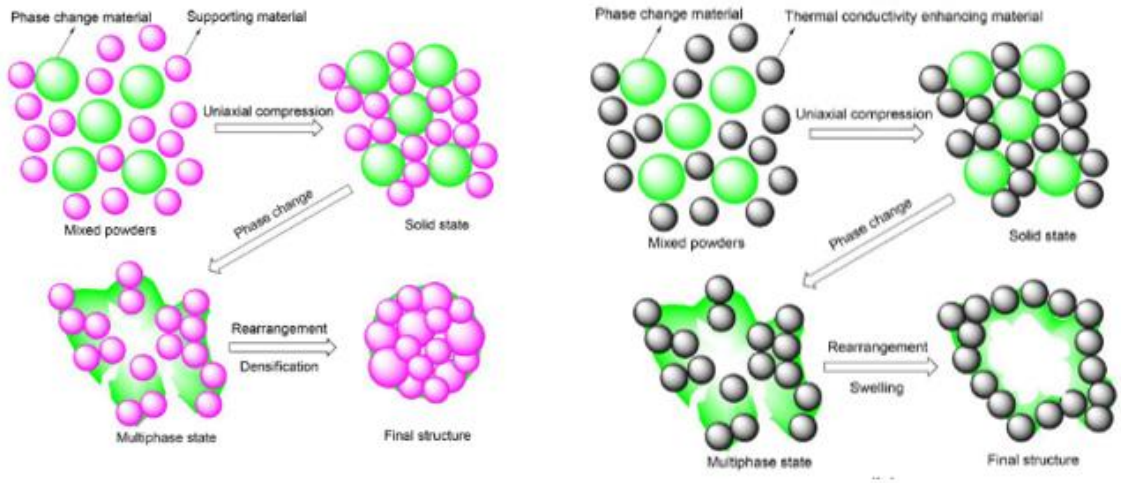

Figure 3-3 **Swelling of Graphite, densification of Vermiculite**

The heat treatment plays in fact the most important role in the fabrication of a shape-stable compressed structure of originally powder-like materials as well as for creating the minimum porosity which allows an even dispersion of the liquid PCM during cycles and a controllable volume variation. The densified skeletonized structure is indeed a result of the bending effect of solidified salt. It is evident that this multi-porous multi-phase microstructure could prevent PCM from leaking, clues suggests that also graphite may take actively part in the holding ability of the created microstructures. The presence of carbon-based component with low wettability which surrounds the salt may increase the PCM probability to be trapped inside pocket-like vermiculite-graphite structures not facilitating the salt leakage.

Figure 3-4 **Bottom view of the composites**

The driving concept revolves around analysing the impact that different contents of PCM solar salt (high and low contents) has on the overall shaped and sintered samples while evaluating different graphite contents, from low, medium to high. Meanwhile, increasing the loading of graphite in the formulations allows to track progressively the extent of the enhancement of thermal properties and to detect if graphite plays a relevant role also from a structural point of view when combined with Vermiculite.

As we can see, after the sintering process some samples exhibit a volume expansion. A certain amount of volume expansion space is necessary to let the salt flow in the matrix and to allow a more controlled graphite swelling. In order to structurally hold the salt while ensuring a minimum porosity for volume variations, when dealing with Vermiculite-based composites is better not to increase too much the holding pressure.

Other important expedients to keep in mind is the well-mixing to allow a complete and more homogeneous sintering and avoid cracking due to areas without the blending effect of the salt and, in addition to this, for this study and according to these conditions, grinding the salt particles increases the leakage probability by enhancing the liquid salt to flow throughout the matrix because it is better mixed.

In studies carried out by Shikui et al[36], a novel approach called dynamic impregnating treatment with vacuuming and supersonic vibration to prepare the PEG/EG composite PCMs was presented. In the project, the novel approach was used to enhance dispersity and absorbability between the supporting materials (GO and SFC) and the phase component (PEG). The structure, thermal properties, and thermal reliability of PCM were also investigated showing that a better dispersion of the PCM in the solid matrix can enhance thermal properties.

3.3 Thermal characterization

The thermal analysis of the study includes the Transient Hot Bridge (THB) for the evaluation of the thermal conductivity.

3.3.1 THB

The instrument adopted is the Linseis THB-500 in the range between -150 and 700 °C. The measurement method is an enhancement of the Hot Wire or the Transient Hot Strip method.

Embedded between two pieces of sample, the sensor emits a heat flow during the measurement. This causes its temperature to rise. The temperature rise over time corresponds to the thermal transport properties of the sample.

3.3.1.1 Sensor type

Sensor type	*Sensor size*	*Thermal conductivity Range*
Sensor THB6N	82 x 42 mm	0.04 to 6 W/mK
Sensor THB6N /MFR	82 x 42 mm	
Sensor THB6K	42 x 22 mm	0.02 to 1 W/mK
Sensor THB6K /MFR	42 x 22 mm	
Sensor QSS	42 x 22 mm	0.1 to 200 W/mK
Sensor Hotpoint	65 x 5 mm	0.02 to 30 W/mK
Sensor Hotpoint HT	300 x 3 mm	

Table 3-4 **Type of sensor fot he THB**

Figure 3-5 **Different type of sensors available: THB6N a), THB6N (MFR) b), THB6K c), THB6K (MFR) d), QSS e), Hotpoint f), Hotpoint HT g)**

The sensor must be covered on both sides by the samples entirely. The surfaces of the sample which are in contact with the sensor must be flat and plane-parallel to get a good thermal contact to the sensor.

The sensor used is THB6K.

3.3.1.2 Setup

Two main parameters for the measurement are chosen, the measurement time and measuring current. The measurement should last until the maximum deviation is exceeded. The current depends on the sample's properties; the temperature during the measurement should rise about 2°C. It is important to know hat above a "critical" heating current value, the measured thermal conductivity drops. The reason for that is the creation of a "turbulent" temperature field, i.e. the produced heat energy cannot be transported by the sample completely anymore.

ΔT is proportional to the measured bridge voltage to a very high degree. So, measuring ΔT allows the calculations of the thermal conductivity λ by:

$$\lambda = \frac{\phi}{2\,\pi\,\Delta T}\,k$$

Where Φ is the applied thermal power, generated by $R_{H,}$ supplied with current and k is a sensor specific calibration factor.

Before the analysis of the samples, the sensor needs a calibration, performed with a sample of a given thermal conductivity.

Some attempts with different current and different time are performed in order to choose a reasonable value of the parameters.

An example of the output is presented.

The temperature dependent material parameters will be extracted by the software from the database.

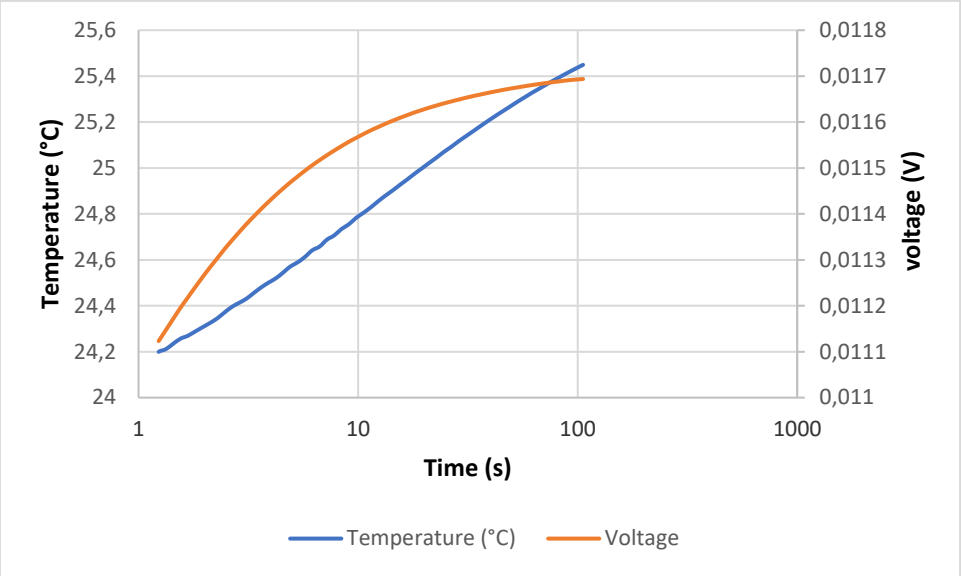

Figure 3-6 **Temperature, voltage with respect to time.**

Ten different attempts have been carried out for each sample in order to choose reasonable value for the current and the measuring time. For each attempt three different measurement are taken with a waiting time of 30 seconds between each measurement.

3.3.1.3 Results

A current of about 90mA and a time of 100s are chosen for the thermal conductivity measurements. The error is ± 2,4%.

50%SS	*TC (W/mK)*	*dif (mm^2/s)*	*70%SS*	*TC (W/mK)*	*dif (mm^2/s)*
SS-V3-0G	0.4816	0.8032	**SS70-V3-0G**	0.4586	0.7936
SS-V1-0G	0.5934	0.7499	**SS70-V1-0G**	0.5538	0.89
SS-V0.25-0G	0.4406	0.7623	**SS70-V0.25-0G**	0.5136	0.6769
SS-V3-10G	0.8473	1.3867	**SS70-V3-10G**	1.2290	1.0281
SS-V1-10G	0.9733	1.276	**SS70-V1-10G**	1.4657	1.98
SS-V0.25-10G	0.7987	1.3777	**SS70-V0.25-10G**	1.3590	1.331

Table 3-5 **Thermal conductivity and diffusivity evaluation**

In the case of 10% of graphite, the thermal conductivity presents higher value in the case of 70% ss with respect to the case of 50% ss. This probably is due to the higher presence of vermiculite.

Due to the methodology of measurement, the thermal conductivity is an average of different configurations. Top-bottom, Bottom-bottom and top-top. An important factor that gives different values for the same sample is due to the fact that in some samples,

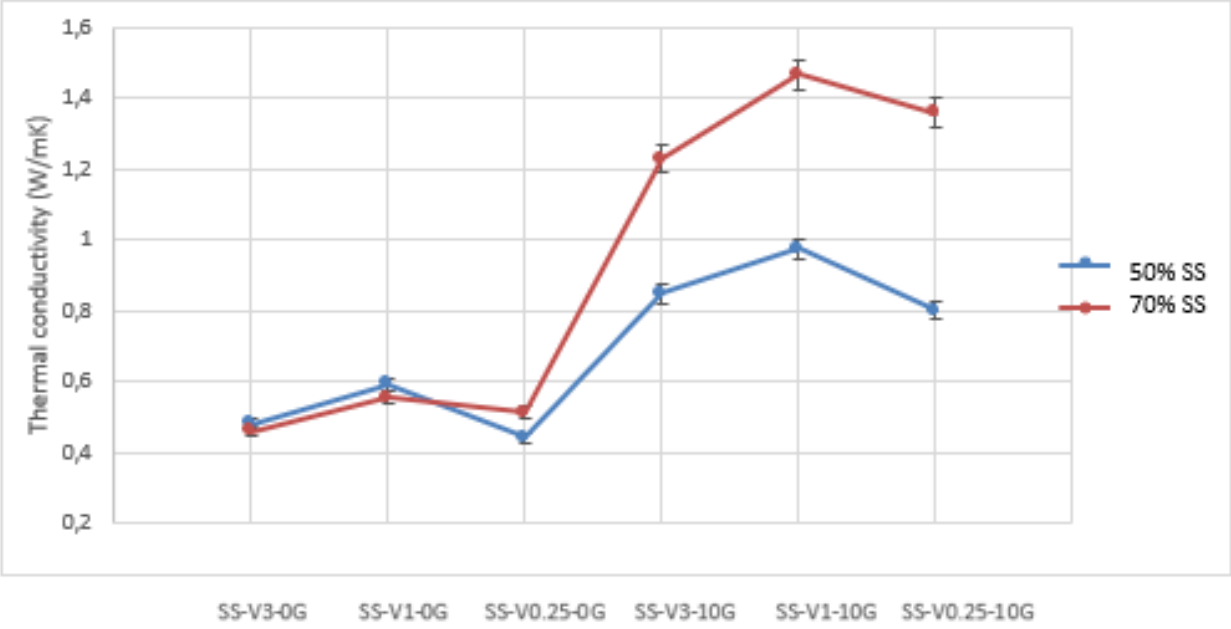

Figure 3-7 **Thermal conductivity**

after the sintering process, leakage was present so that at the bottom of the composites an increasing quantity of salts is present with respect to the top.

In the table below are reported the values of thermal conductivity for the materials considered in the analysis.

Materials	Thermal conductivity [W/(m*°C)]
Solar Salt ($60\%NaNO_3$:$40\%KNO_3$)	0.45±0.067 0.52
Vermiculite	0.04-0.12
Graphite	25-470

Figure 3-8 **Thermal conductivity of materials used** [37]

Thermal conductivity enhancement by means of carbon-based particles or microstructures is one of the most debated issues when dealing with composites at a micro-scale perspective but is one of the key parameters which can lead to overwhelmingly increased thermal performance at a device-scale. Even though Graphite contribution has nothing to do with latent heat potential of the SSPCM (the PCM is the only contributor to that), it has a great impact on gaining higher heat transfer rates allowing charging/discharging processes to reach the equilibrium temperature in less time. Thermal enhancement through the addition of carbon-based components/fibres/nanoparticles or Expanded Graphite/foams have been widely recognized in the composites experimental research.

In order to achieve a high thermal conductivity is fundamental the presence of a carbon network. The optimum is for a vermiculite size of 1 mm.

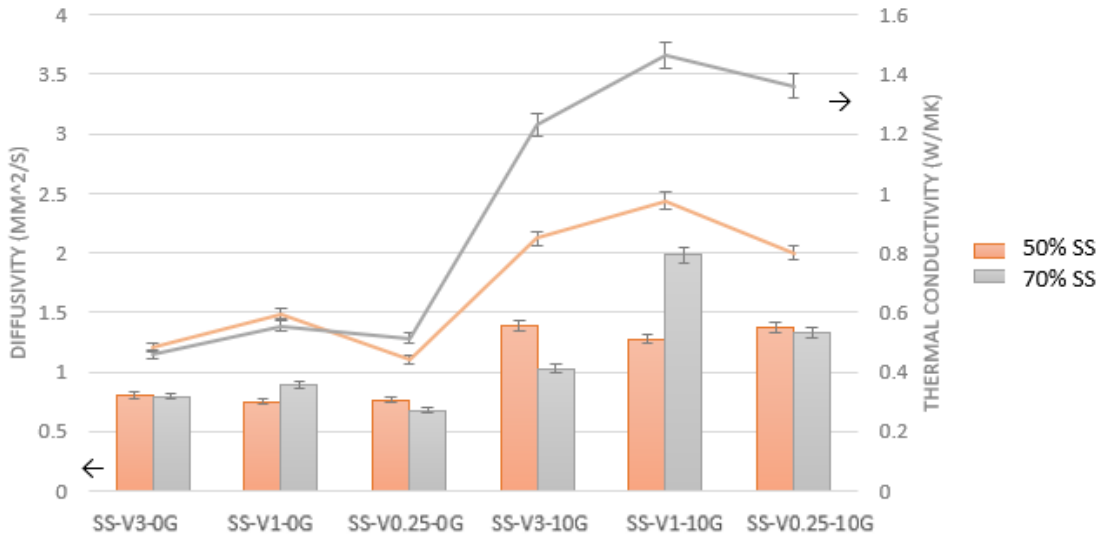

Figure 3-9 Diffusivity evaluation for all the samples

The evaluation of the thermal diffusivity is also given by the transient hot bridge.

A different behaviour can be seen in the cases of 50% of SS and 70% of SS.

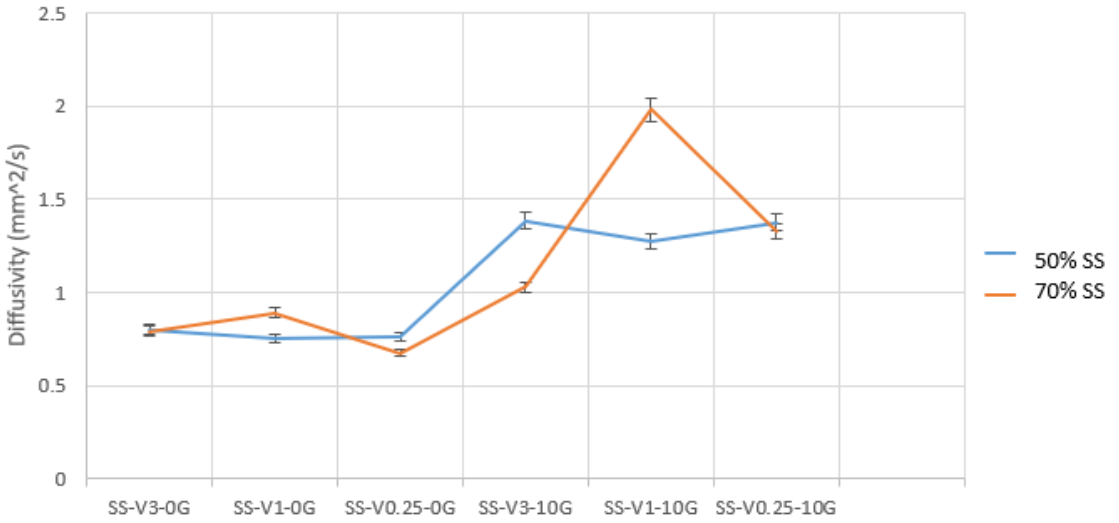

Figure 3-10 **Thermal diffusivity**

Smaller particle size leads to lower interparticle distance and more chances for the formation of thermal conductive 'pathway'[38]. As in the case of the thermal conductivity better results are obtained for a particle size of 1 mm. An opposite situation occurs for composites with 50% of solar salts.

3.4 Physical properties

3.4.1 Density and porosity measurements

There are different measures of density that sometimes may lead to real conceptual mistakes. On one hand there is the bulk (or envelope) density while on the other hand there is the effective (actual, real, apparent or skeletal) density. The effective density provides an estimation of the actual mass of the sample divided by its volume without accounting for the pore space. This density is the one usually compared with the theoretical density and, for a porous material, it's higher than the bulk one. Bulk density on the other hand, is the measure of density related to the sample's bulk volume taking into account also the volume of the pores. It provides usually an underestimation of the actual volume, but it may be useful to evaluate properties like porosity and thermal conductivity of composites.

While on one hand the density measurements of a solid and rigid sample are a straightforward task, measuring density of composites with irregular size should be more carefully addressed. The latter can in fact include cracks, pores tortuous passageways and may lead in some cases to inaccurate results.

In order to have a preliminary estimation of the porosity of the green pellets, and to have an idea about how pore formation affects the composites bulk volume, the

measurement of the bulk density is fundamental. As previously mentioned, the bulk density is a measure of the volume density when including the pore volume.

$$\varepsilon = 1 - \frac{\rho_{bulk}}{\rho_{actual}}$$

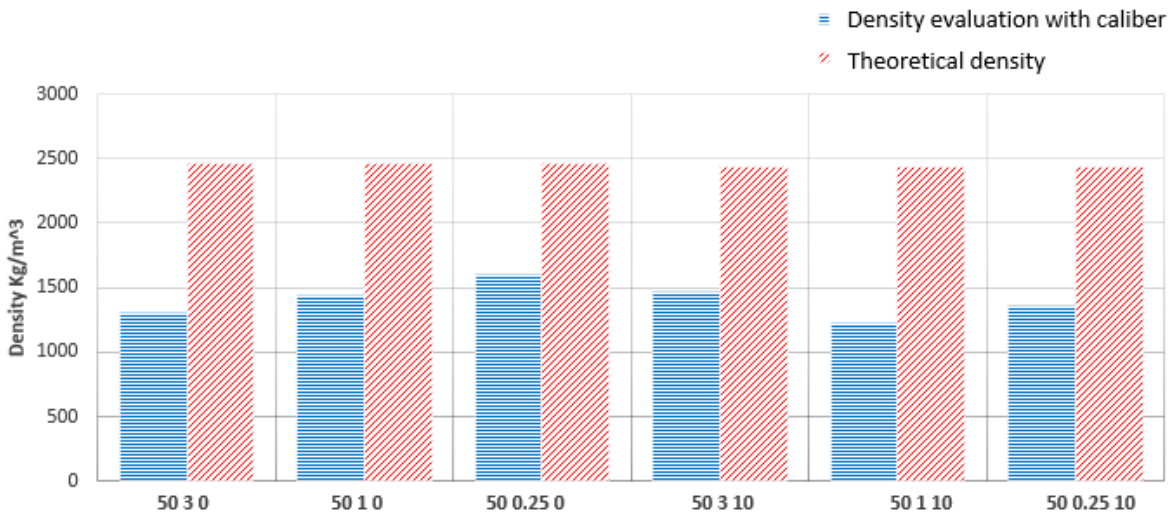

Figure 3-11 Density of the samples with 50% of Solar Salt with and without graphite, with different Vermiculite's particles size

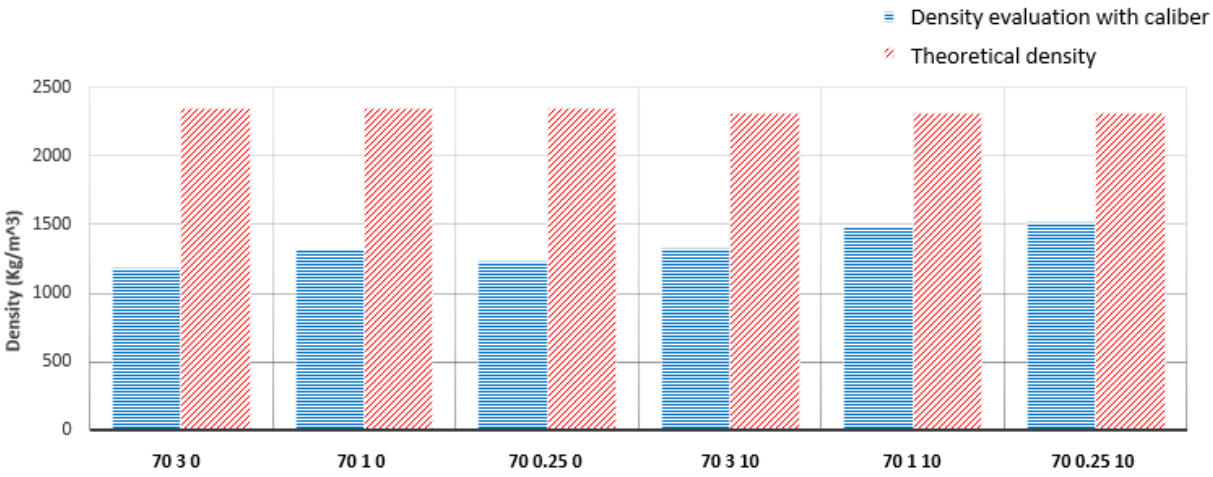

Figure 3-12 Density of the samples with 70% of Solar Salts with and without graphite, with different Vermiculite's particles size

Theoretical density results to be much higher than the bulk one, therefore a high porosity is expected. When comparing the two subsets of formulations, the 50%-PCM set shows higher density values due the higher Vermiculite contents, the 3 mm particle size contribute to the formation of slightly bigger pellets because of the high void volume occupied by the casual arrangement of the Vermiculite particles across the skeleton.

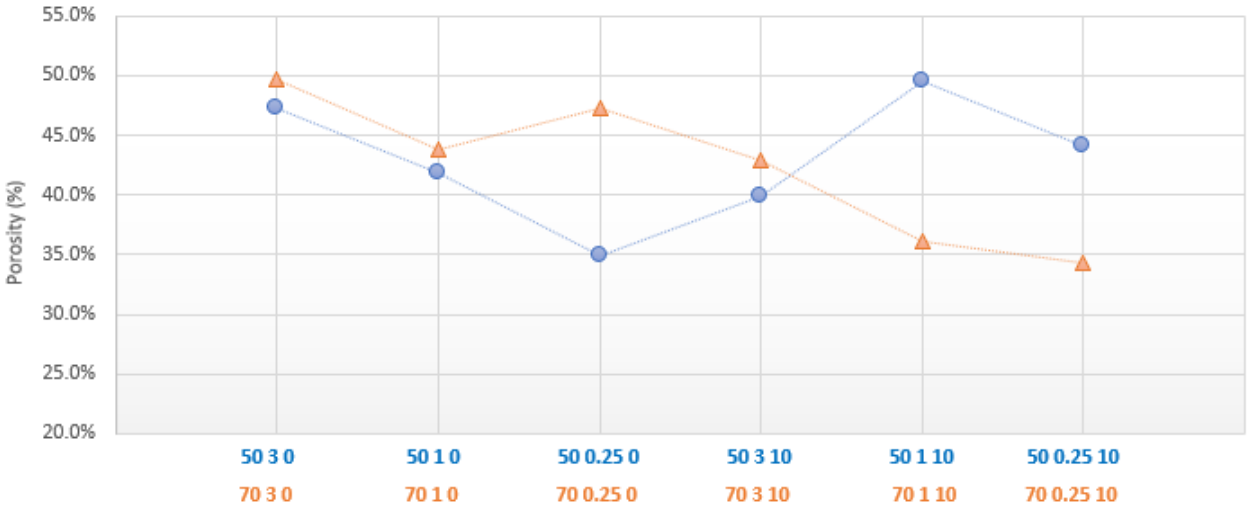

Figure 3-13 Porosity measurements considering the bulk densities obtained by calibre and weight measurements of the pellets.

For highly porous composites like the manufactured green pellets this specific kind of sintering (occurring at lower temperatures) is the result of pore rearrangement and the compacting effect of the Solar Salt in the liquid phase. The high content of porosity can be linked with the leakage resulting after the sintering process. Solar Salts particles leaking from the pellets leave behind them empty spaces. The powder-like particles during the heat treatment start to densify and to form necks and interconnected passageways to reach a compact structure as shown in Stage III. The only missing point that distinguishes this particular sintering process pushed to 300°C with respect to the actual sintering of ceramics shown in Figure (up to >1000°C) is the final stage where the isolation of pores occurs due to the grain growth and diffusion phenomena occurring at higher temperatures.

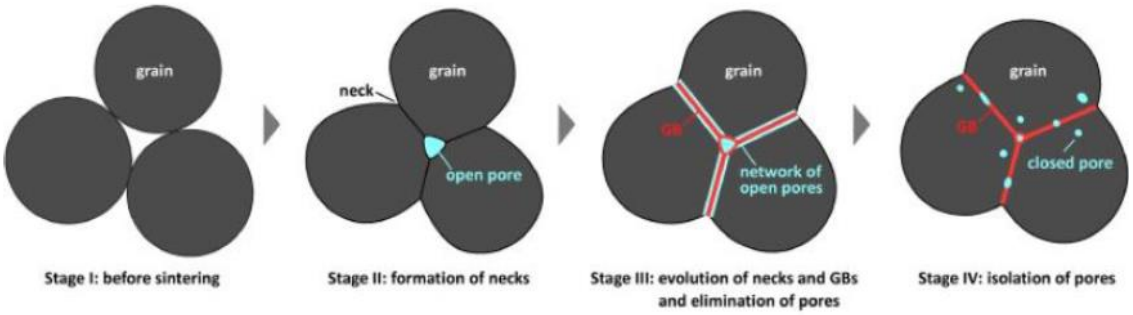

Figure 3-14 Sintering stages of ceramics[39].

3.5 Complementary micro-structural analysis

The investigation of SSPCM microstructure to track the relationships between structure properties, thermo-physical properties and overall performance of the material has been carried out. A microstructural analysis has been conducted taking advantage of X-Ray micro-tomography.

3.5.1 XRT

The equipment used is the multiscale X-ray tomography SkyScan-2211 which allows a 3D non-destructive analysis of the samples and of their internal reconstruction in the range between >200mm to sub-micron level. The system used is composed of an X-Ray source and two X-ray detectors one for large or highly dense objects and another for smaller specimens. The X-ray tomography is a widely used technique for non-invasive analysis in the medical field but also for other industrial purposes.

As shown in Figure below, the functioning principle is based onto cone beam reconstruction where a cone-shaped beam is emitted by an X-Ray source onto a sample placed in the middle of the trajectory from the source to the 2D detector.

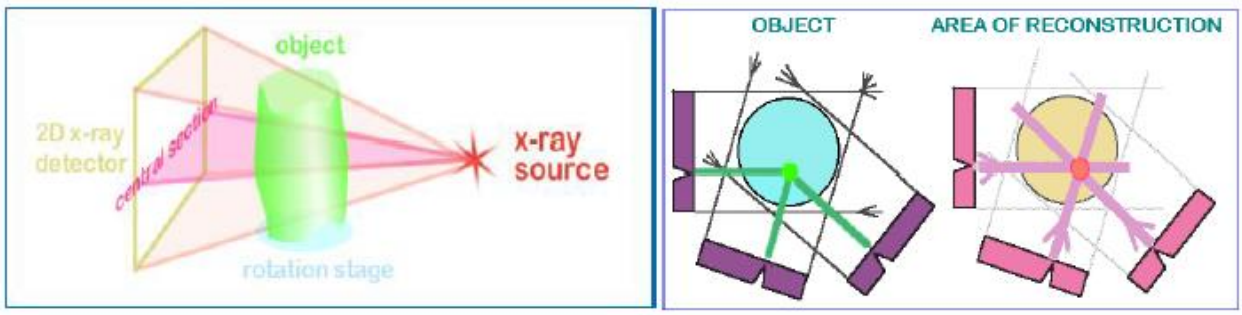

Figure 3-15 Functioning principle of X-Ray Tomography (left). Reconstruction technique of the digital images from the XRT (right).[40]

Ever since the 3D specimen is invested by the beam the detector collects shadows out of it producing the first two-dimensional reconstruction. Every point in the shadow image of the object produced can be considered as carrying information about the absorption of the 3D object which is in the trajectory of the partial X-Ray beam. Each point of the 2D representation is allocated into the computer memory as a pixel corresponding to the possible displacement of the object, the following reconstruction of the same object must be in the same field of view. Thanks to the rotation of the stage holding the sample several 2D reconstructions are produced and, as far as the shadows are collected from different rotation angles, the actual localization of the absorption point of the beam is registered. During this process, and according to the rotation speed and steps, the projection and reconstruction area decreases to a single object point, this operation is called "back-projection". The increasing number of shadow projections collected from different views produces a more precise localization of the absorption point and the more is possible to obtain higher quality images.

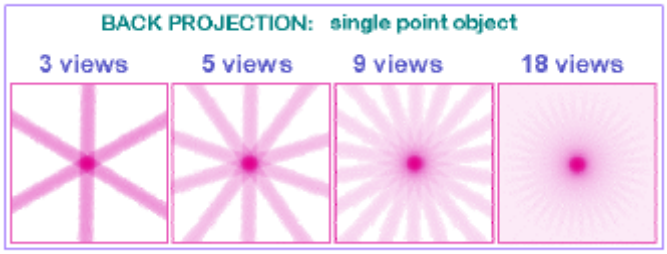

Figure 3-16 Detail on single point object reconstruction.[40]

When the acquisition is finished the reconstruction can be started. The obtained shadow angular projections will be used for the reconstruction of the virtual slices through the object. A raw data cross section is then generated using the reconstruction algorithm. This raw data is not yet an image; it is a matrix of numbers corresponding to absorption values in the reconstructed cross section. The size of the reconstructed array NxN is defined by the number of pixels in the lines of the angular projection images N.

Complementary software should be used to complete the analysis and to provide a quantitative evaluation of the structure of the specimen. A summary of the main steps which have been followed is listed into the diagram below.

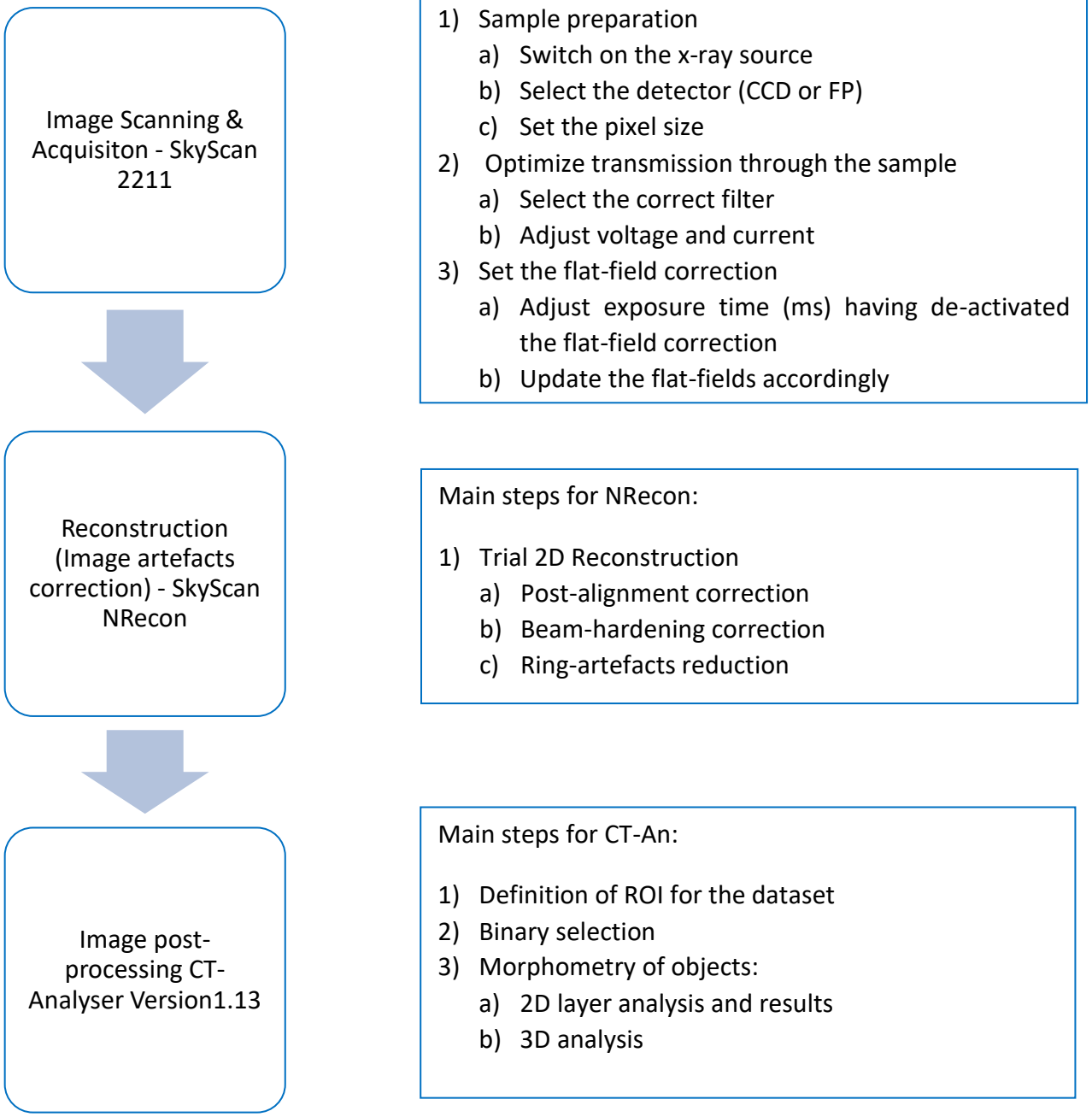

As a reference in the following table are listed the conditions for the scanning of the samples.

[Acquisition] properties:
Source Voltage (kV) = 100
Source Current (µA)= 200
Source focus mode =Micro focus
Number of Rows = 1536
Number of Columns = 1920
Image Rotation =0.0790
Exposure (ms) = 100
Image Pixel Size (µm) = 9.95
Scaled Image Pixel Size (µm) = 9.95
Object to Source (mm)=38.125
Inclination in lifting(µm/mm) =0.919
Vertical Object Position (mm) =26.000
Filter=No filter
Depth (bits)=16
Rotation Step (°) =0.200
Use 360 Rotation =YES
Type of Scan =Flat-Panel
Estimated scan time =00h:39min

Figure 3-17 **Acquisition conditions**

3.5.1.1 Digital Image post-processing for micro-structural investigation

Image post-processing methods include filtering technique in images as well as pixel-based neighbouring algorithms allowing a connection with physical microstructural properties. A few reconstruction parameters have to be adjusted manually in a try-and-error fashion using the preview function. With NRecon software it is possible to adjust one parameter at a time, while keeping all other parameters fixed. In this way, it is possible to tune 3 parameters: post-alignment, beam-hardening correction, ring artefacts.

Post-alignment compensates possible misalignment during acquisition. Wrong alignment compensation would cause tails, doubling or blurring in the reconstructed image.

Beam-hardening correction compensates beam-hardening effect by linear transformation in the software. Depth of correction can be selected according to object

density. Same as the post-alignment this parameter needs manual adjustment by visualizing the resulting images.

Ring artefacts reduction is applied on the projection before any other processing steps.

After the reconstruction, the data are analysed through CTAn software in order to quantify micro-structural properties, to obtain a volume reconstruction and to tackle the structural evolution layer by layer with the aid of a Volume of interest selection. The VOI is a reduced 3D domain allowing to include into the study only the relevant areas or to eliminate defects resulting from the acquisition phase or excessive irregularities which may lead to a non-representative volume or overestimated values of porosities.

Parameters of interest which can be extracted from the post-processing analysis of the digital images are 2D areal porosity, 3D open and closed porosity, pore size distributions and many other information.

After a reconstruction obtained with NRecon and CTAn a postprocessing of the data has been carried out with the use of MATLAB to analyse the porosity and tortuosity with algorithms able to allow a connection with physical microstructural properties from a greyscale image (resulting from the reconstruction) to binary image (obtained after the postprocessing with MATLAB).

Otsu's method, is used to perform automatic image thresholding. In the simplest form, the algorithm returns a single intensity threshold that separate pixels into two classes, foreground and background.

The main purpose for this category of algorithm is to perform neighbouring pixel operations while maintaining the basic connectivity of the image patterns. The main connection between these pixel-based operations and the physical properties of the samples is based on the assumption that pores are actual micro-structured pathways able to hold and transport the melting salt. Such algorithms allow to simplify the micro-structural study without altering the image patterns.

There is the possibility to correlate the porosity to the thermal conductivity.

As an example, we can consider the case of the composites with 70% of SS, 10 % of graphite and vermiculite size of 3mm and 0,25mm. In the two cases the higher thermal conductivity is for the vermiculite size of 0,25 mm (6% bigger than the second case), this could be caused by the higher porosity in the case of 3mm vermiculite.

The obtained reconstruction 2-D binary images and 3-D rendering of the two cases are presented. The higher porosity can be explained considering that after sintering process, lower size of vermiculite is able to rearrange giving rise to lower empty space.

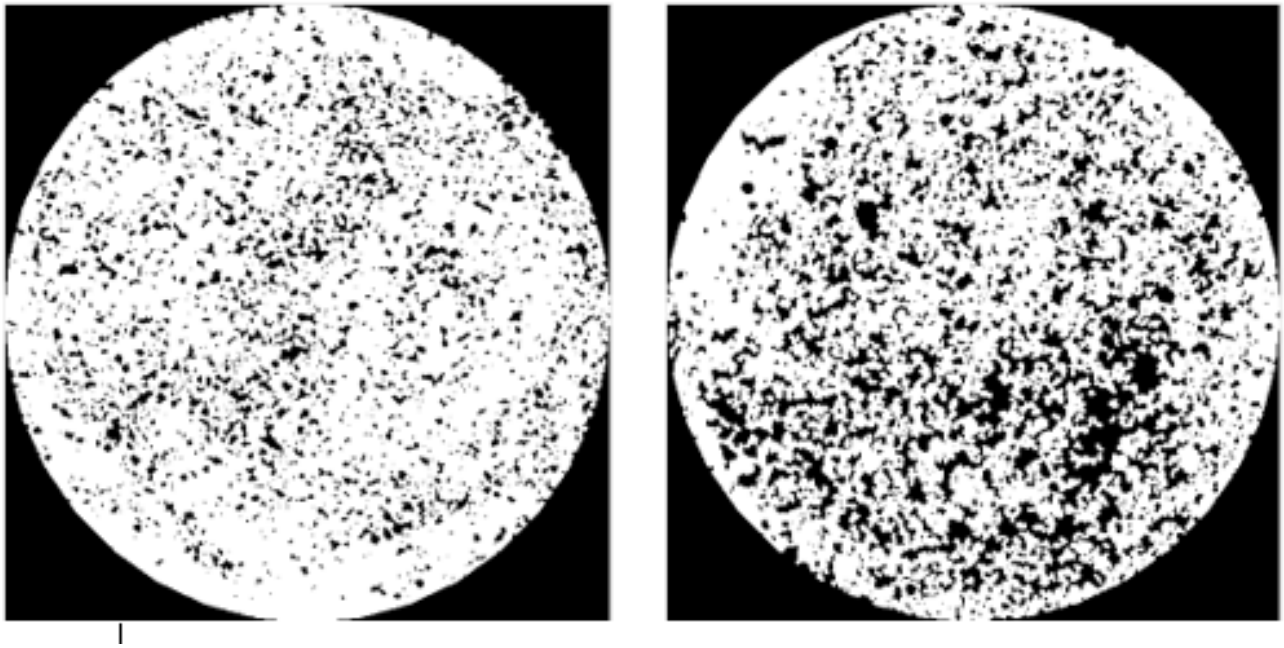

Figure 3-18 a) composite with 70% of solar salts 10% of graphite and vermiculite size of 0,25 mm-0,25 b)composite with 70% of solar salts 10% of graphite and vermiculite particles size of 3mm

In the second sample the higher porosity is evident.

A different situation is present in the case of composites of 50% of SS, 0% of graphite and vermiculite size of 0,25mm and 3mm. In this case the thermal conductivity is 9% higher for the composite with 3mm of vermiculite.

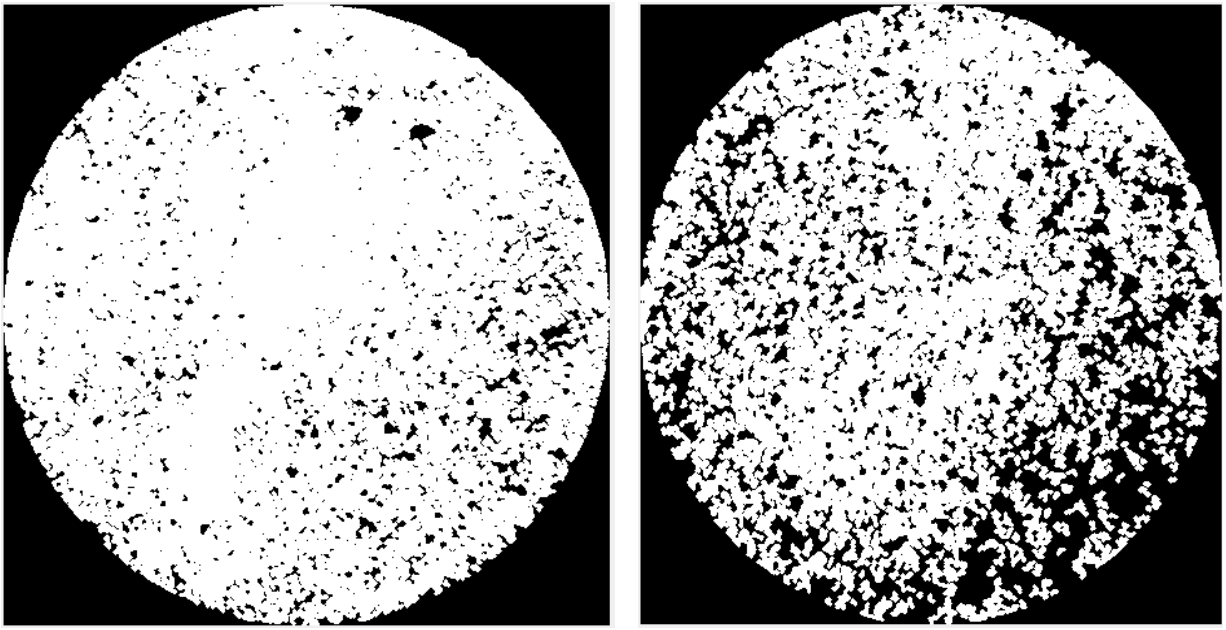

Figure 3-19 a) a) composite with 50% of solar salts 0% of graphite and vermiculite size of 0,25 mm-0,25 b)composite with 50% of solar salts 0% of graphite and vermiculite particles size of 3mm

Even if in the second sample the porosity is definitively higher, the thermal conductivity is higher. The analysis should go further, considering the percentage of open and closed porosity.

For each z position the open porosity is plotted for both the composites.

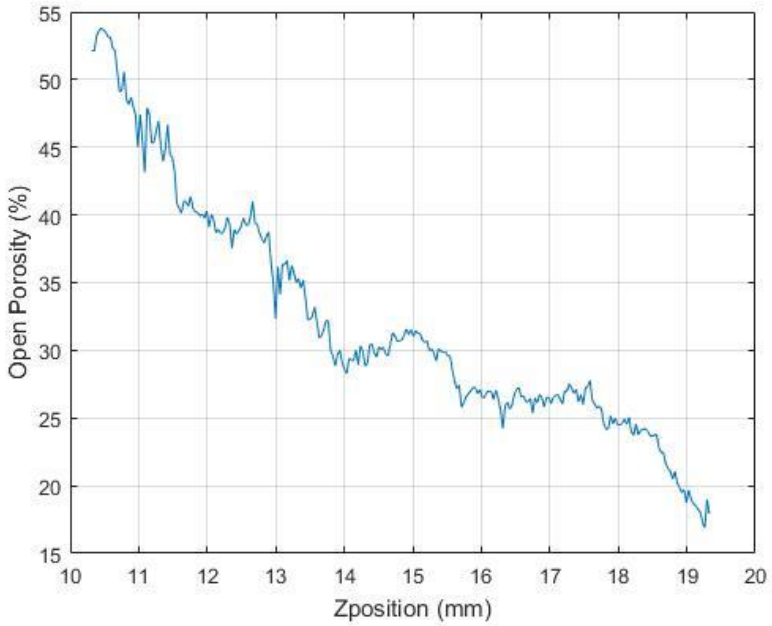

Figure 3-20 Open porosity for 50-0-3

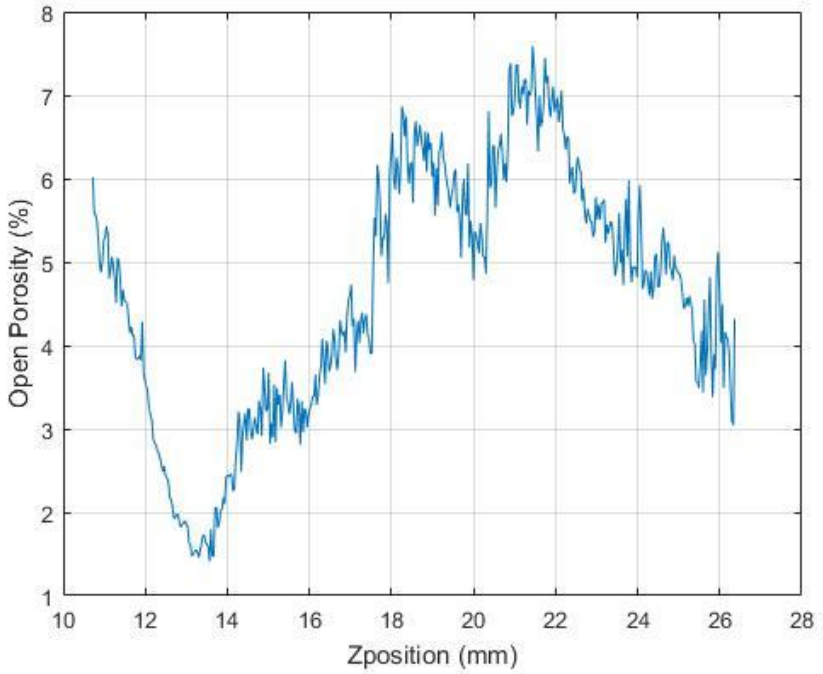

Figure 3-21 Open porosity for 50-0-0.25

Although the total porosity is higher for the case with 0,25mm of vermiculite, the percentage of the open porosity is small (little number of interconnected pores), meaning that if the solar salt is not present in that pore, only air is present thus reducing the conduction. In addition to this we have to mention that in the case of 0,25 mm there was a large amount of leakage resulting in an increasing presence of solar salts at the bottom of the sample.

As an example, a representation of reconstruction is reported. In the figure below faces of the sample are depicted from top to bottom.

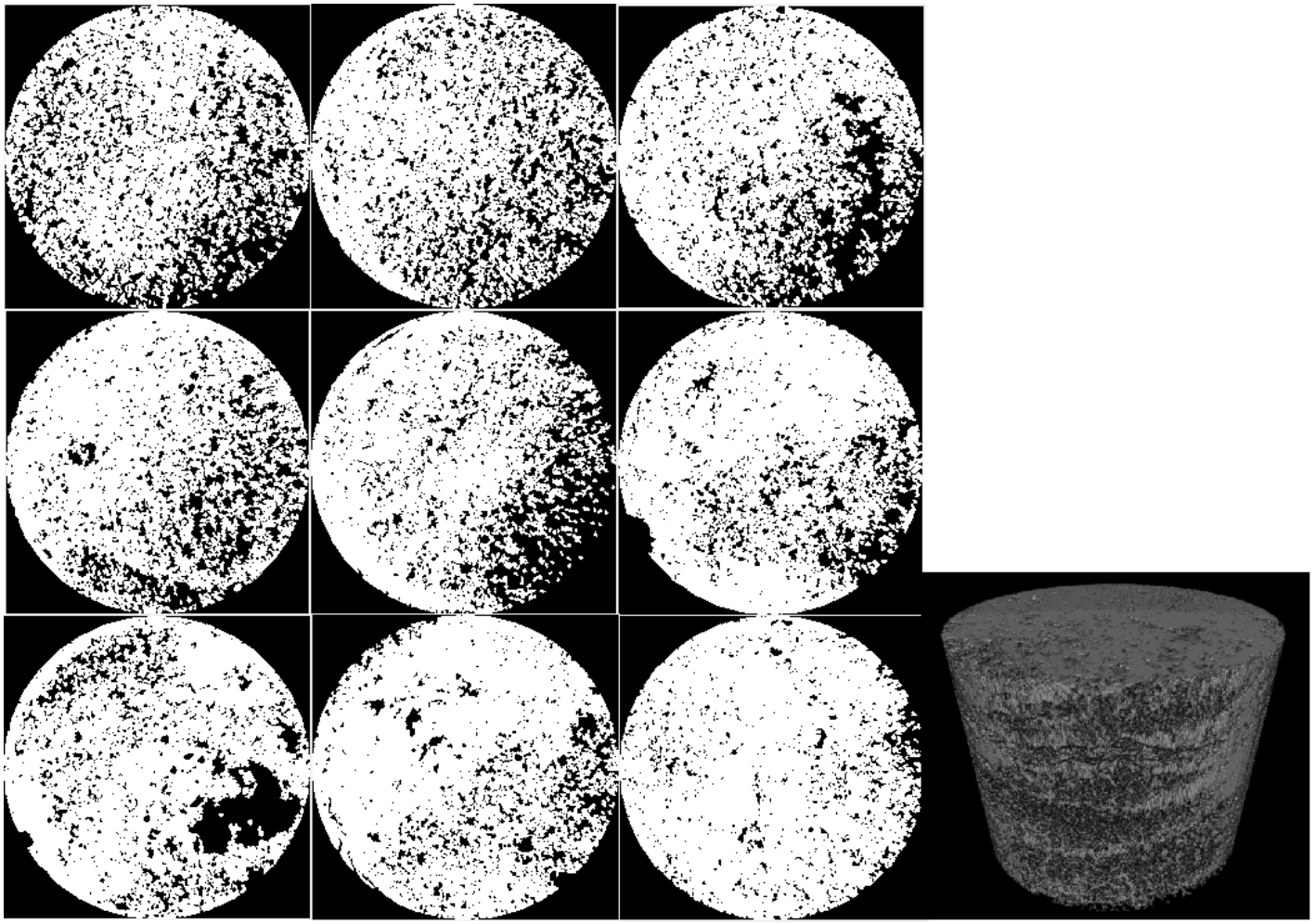

Figure 3-22 the evolution of the 2D slices from top to bottom layers of the sample 50-0-3 and volume reconstruction

The evaluation of the porosity is plotted along the z position. Due to the failure of the leaking test we can see that salts leaking from the sample give rise to open pores at the top of the composite and less porosity is encountered in the bottom section.

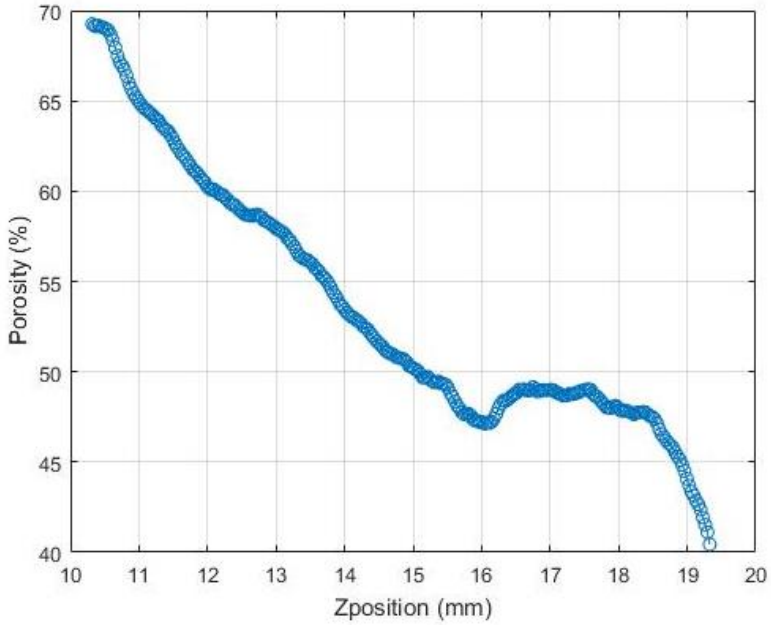

Figure 3-23 **Porosity along the z position**

An important consideration can be applied analysing a section in the xz plane.

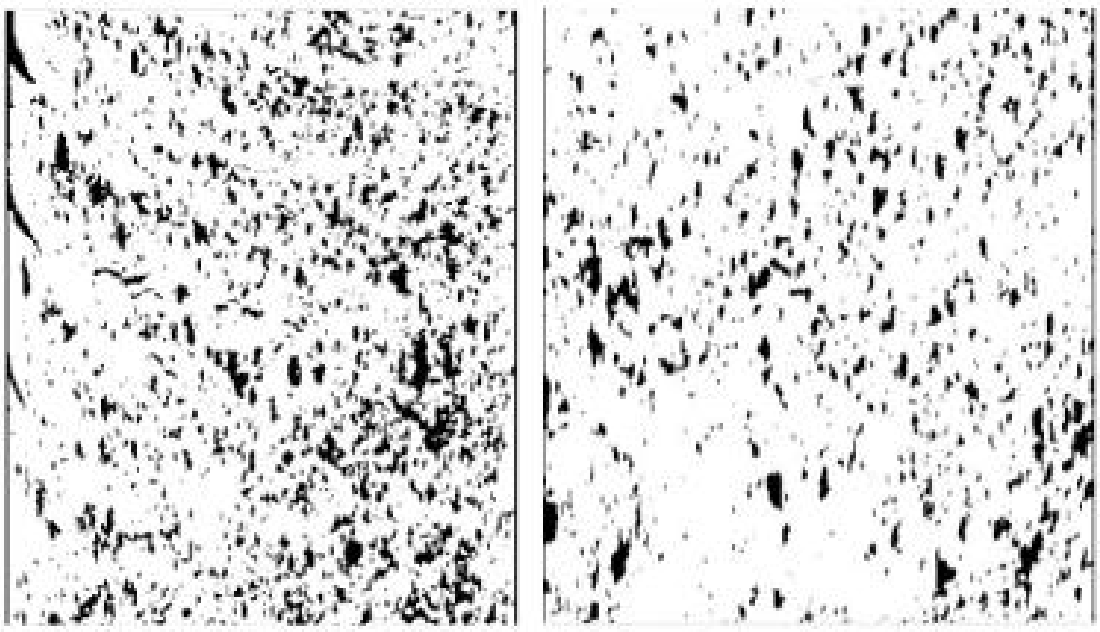

Figure 3-24 **xy projection for 70-10-3 and 70-10-1**

In the first case the higher amount of porosity interrupts the network, consequently the thermal conduction from top to bottom is lower than in the second case.

4. DYNAMIC SIMPLIFIED MODEL FOR SSPCM

To improve the thermo-physical property and mechanical stabilization of SSPCMs, various PCMs and supporting materials have been widely investigated[41].

It is essential to estimate the thermal performance and energy saving benefits in the design and optimization of PCMs. To predict the thermal performance accurately, the thermal models for PCMs have been increasingly studied in recent years. Alawadi[42] et al. developed a two-dimensional thermal model for PCM in building brick wall with the effective heat capacity method. The model was solved by using finite element analysis method and showed good effectiveness.

Mirzae et al.[43] proposed a new one-dimensional analytical model for PCM plate based on RC-circuit concept. The performance of the model is well for a single melting or solidification process. Dynamic simplified models with resistance and capacitances are widely used in conventional walls or planes. The resistance and capacitances for conventional model is constant and is not affected by the environmental conditions.

4.1 Description of the model

Numerical PCM model needs meshing the ssPCM slab with many nodes or computational domain.

In this model Bi number is determined in order to understand if the lumped parameters can be used for transient heat transfer calculation. In this study Bi number is below the suggested threshold of 0.1. It matches the Bi number criteria.

For the model some assumptions are made as follows:

- Phase transition process of SSPCM occurs in the range of solidification temperature and melting temperature.
- As initial condition, the temperature is considered to be uniform
- The thermal conductivity is supposed to be constant with temperature
- The results presented are independent on surface area.

Under these hypotheses the 1D conduction equation is written

$$\rho c_p \frac{\partial T}{\partial t} = k \frac{\partial^2 T}{\partial x^2}$$

For what concerns the time discretization, the implicit backward Euler (BE) method is used. Being an implicit method, to obtain the solution after a time-step Δt we have to solve a non-linear equation. This is evidently much more time consuming, but it is stable.

Central finite-difference scheme is adopted as a spatial discretization scheme because it is second-order accurate.

In a discretized form it is possible to write:

$$-aT_{i+1}^{n+1} + (1+2a)T_i^{n+1} - aT_{i-1}^{n+1} = T_i^n$$

Where index i correspond to the space discretization, index n corresponds to the time discretization and a is defined as

$$a = \frac{\alpha \Delta t}{\Delta x^2}$$

α is the thermal diffusivity.

The capacitance of the system is considered to be variable with the temperature in order to consider the phase change of the material during the simulation; a Gaussian expression can be adopted. In particular is assumed to be C=ρ c V where c is

$$c(T) = \frac{c_{p,s} + c_{p,l}}{2} + \frac{L}{\Delta T_{SL}\sqrt{\pi}} e^{-\frac{(T-T_{av})^2}{\Delta T_{SL}{}^2}}$$

where cp is the specific heat of the solid (or liquid) PCM, ΔT_{SL} is condensing/melting temperature range and T_{av} is the average temperature in the phase change range and L is the latent heat.

Considering a material with a phase change around 27°C the evolution of specific heat function of temperature is plotted as an example.

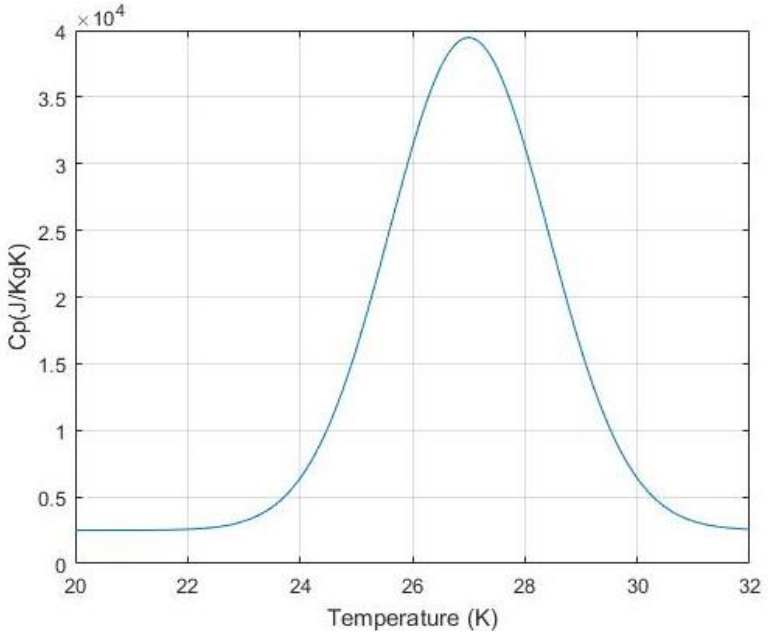

Figure 4-1 Specific heat function of temperature

On the left boundary an imposed temperature is considered whilst on the left boundary a Robin boundary condition is applied to consider the convective loss toward the ambient.

5. ENERGY HARVESTING

5.1 Thermoelectric energy harvesting

Some ways of using waste heat sources are known; thermoelectric is one of the latest technologies. In 1821 the German physicist Thomas Johann Seebeck discovered that when two strips of different electrically conducting materials were separated along their length but joined together by two "legs" at their ends, a magnetic field developed around the legs, provided that a temperature difference existed between the two junctions. Thermoelectric Generators (TEGs) based on the Seebeck effect directly convert heat into electrical energy without moving parts which facilitates their implementation and reliability. At the atomic scale, an applied temperature gradient causes charge carriers in the material to diffuse from the hot side to the cold side. A TEG module is made of p- and n-type semiconductor elements that are electrically connected in series, to generate a higher voltage, and thermally in parallel to keep each semiconductor element at the same thermal gradient. These elements are typically arranged in a planer array and sandwiched between two thermal ceramic plates. The physical effects taking pi ace in a TEG are the thermal conduction and the Seebeck, Peltier, and Joule effects. Peltier effect, the cooling of one junction and the heating of the other when electric current is maintained in a circuit of material consisting of two dissimilar conductors; the effect is even stronger in circuits containing dissimilar semiconductors.

The main advantages of electric current generation by thermo elements are the following[44]:

- The lack of refrigerant and lubricating oil, which puts thermoelectric devices in a series of future-oriented solutions for protection of the environment.
- The lack of moving parts contributes to operating cost savings related to time required for repair and maintenance (a broken thermocouple can be exchanged for a new one in short time).
- Possibility to maintain a constant operating temperature of thermocouples with a small deviation of ±0.1K.
- Possibility to adjust the range of cooling capacity between 0 and 100%.
- A simple, maintenance-free structure.
- Possible different shapes of thermocouples – they may take the form required for a particular application.
- Possibility of cooling only the selected area or component of a device or machine.
- Operation without noise emission.
- Possible operation in conditions of weightlessness and at high load, which is important in military and space applications.

Depending on size, energy source and application, the output power for energy harvesting devices is typically in the range between microwatts and hundreds of mill watts[45].

The primary limitation of the thermoelectric power generation is its relatively low conversion efficiency, that depends largely on the available temperature difference ($\Delta T = Th - Tc$) across its hot and cold sides.

High electrical conductivity, low thermal conductivity and high Seebeck coefficient are desirable in order to maximize TEG's figures of merit. Research is also working in the design of optimized electronic circuit interfaces to extract the maximal electrical power *P* to the connected load.

A heat storage unit can be employed to transform a temperature variation in time into a spatial temperature differenceΔT, which can then be exploited by a TEG. A material that changes phase within the ambient temperature variation range (PCM) is used in the HSU to achieve a large energy storage density, as well as to maximize the average temperature difference.

5.1.1 Description of the device

The HSU comprises a PCM in thermal contact to the TEG. When the environmental temperature fluctuates, heat flows in and out of the HSU. The energy output of the harvesting device can be collected, stored and distributed by a power management system.

In the selection of the PCM, phase change within the available temperature range must be ensured. The specific heat capacity cp and phase change energy should be maximized. High thermal conductivity is required to minimize temperature gradients within the PCM. For this purpose, additives to enhance k may be essential.

Good thermal contact with the TEG is necessary.

A TEG with low thermal conductivity is desirable, should be much lower than the thermal conductivity of the PCM to maximize the ΔT applied to the TEG. Furthermore, depending on the ambient temperature cycle profile, a low k is beneficial as it increases the time lag between exterior and interior temperature change.[45]

A dimensionless figure of merit (ZT) is defined as a symbol of the thermoelectric performance[46]:

$$ZT = \frac{\alpha^2 \sigma}{k} T$$

Conceptually, to obtain a high ZT, both Seebeck coefficient α and electrical conductivity σ must be large, while thermal conductivity k must be minimized. The Wiedemanne-Franz law requires the electronic part of thermal conductivity (k) to be proportional to electrical conductivity (s), and the Pisarenko relation limits the simultaneous enlargement of α and σ.[46] Thus reducing thermal conductivity is an effective method to enhance thermoelectric performance.

The theoretical maximum efficiency can be written as a function of ZT and the temperature difference (ΔT=$T_h - T_c$) across its hot and cod side [46]:

$$\eta = \frac{T_h - T_c}{T_h}\left[\frac{\sqrt{1+ZT}-1}{\sqrt{1+ZT}+\frac{T_c}{T_h}}\right]$$

Generally, the maximum power output for TEG is given by[47]:

$$P_{max} = \frac{(S\,\Delta T)^2}{4\,R_{in}}$$

where S is the Seebeck coefficient of the thermoelectric device which is dependent on the Seebeck coefficient α of the thermoelectric materials and pairs of thermocouples in the device. $R_{in}$is the internal electrical resistance of TEG.

In order to enhance the figure of merit of a thermoelectric material, some attempts were done by Zhang et al.[46] increasing the Seebeck coefficient by doping the material with impurities. As an example, Na doped PbTe with the same carrier concentration, Tl doped PbTe shows increased effective mass and pronounced higher Seebeck coefficient.

5.1.2 Model description

When the temperature fluctuates, heat flows in and out through TEG, resulting in generation of electrical energy.

The approach considered is neglecting the contact thermal resistances. The TEG model includes a constant voltage source which is proportional to the difference of temperature at the sides.

The electrical power supplied to the load is defined by:

$$P = V_{oc}I - RI^2$$

The maximum energy that can be harvested from a heat storage device can be calculated, for a given ambient temperature sweep, from the total available heat energy and the maximum possible TEG efficiency. For this calculation, zero heat leakage and a linear approximation of η is used:

$$\eta = \gamma \, \Delta T$$

The operation with a small ΔT results in a low thermal conversion efficiency[44].

The maximum energy that can be harvested by a heat storage thermoelectric harvester of heat capacity C and latent heat L, from an ambient temperature cycle of change θ, is[45]:

$$E = \int_{t_{in}}^{t_{fin}} P \, dt$$

For a given application and temperature cycle, the total available energy will depend on the PCM properties and mass. Low thermal conductivity is the main issue that affects the heat flow dynamics.

For the model with no contact thermal resistance, the equation of the electrical power is a parabolic function having roots in the presence of a short-circuit *(I = Isc= V_{oc} / R),* or an open circuit *(I* = 0). Locating the MPP versus load current *I* is obtained by putting the derivative of this electrical power equal to zero:

$$\frac{dP}{dI} = V_{oc} - 2RI = 0$$

Which gives the optimum current:

$$I_{MPP} = \frac{V_{oc}}{2R}$$

This optimum current leads to the maximum electrical power by replacing its expression above:

$$P_{max} = \frac{V_{oc}^2}{4R}$$

Similarly, locating the MPP versus output voltage *Vo* is obtained by putting the derivative of the electrical power equal to zero:

$$\frac{dP}{dV_o} = \frac{V_{oc} - 2V_o}{R} = 0$$

Thus, the output voltage of the TEG at the MPP is given by:

$$Vo_{MPP} = \frac{V_{oc}}{2}$$

The output voltage Vo_{MPP} and the load current I_{MPP} at the MPP are linked by the following equation:

$$Vo_{MPP} = R_l \, I_{MPP}$$

which is equivalent to:

$$\frac{V_{oc}}{2} = R_l \frac{V_{oc}}{2R}$$

Consequently, it can be seen that in the simplified TEG model, the MPP is achieved by putting an equivalent load value equal to the TEG's internal equivalent electric resistance.

5.1.3 Material selection

A thermoelectric material has a specific temperature at which the conversion efficiency is at its maximum. Thus, when working in a temperature range, the material often operates below its potential maximum performance. To increase its performance, a TEG can be segmented with materials optimized for different temperature ranges. Commercially used thermoelectric materials can be divided into three groups:

• low temperature materials, up to about 250°C, (e.g., materials based on bismuth telluride)

• intermediate temperature materials, up to about 600°C, (e.g., materials based on lead telluride)

• high temperature materials, up to about 1000°C, (e.g., silicon germanium alloys)

Parameter[48]	**Value**
Seebeck coefficient α	$2.2\text{x}10^{-4}$ V K^{-1}
Heat conductivity k	1.5 W $m^{-1}\,K^{-1}$
Internal resistivity ρ	$1\text{x}10^{-5}$ Ωm^{-1}
Thickness e	$1\text{x}10^{-4}$ m
ZT	0.8

Table 5-1 **Thermoelctric material properties**

RT28 (a mixture of paraffin) is a kind of suitable phase change material in low temperature applications due to the phase change temperature (about 27°C) and high

latent heat of fusion[49]. EG is used to enhance the thermal conductivity and shape RT28. To perform good stability, the feasible mixing weight ratio of RT28 and EG is 8:2[50].

Items[50]	Value
Material	RT28/EG
Density	750 kg m^{-3}
Latent heat	160200 J kg^{-1}
Phase-change temperature	26.9-28.9 °C
Specific heat	1980 J $kg^{-1}K^{-1}$
Thermal conductivity	9.5(s)/9.8(l)W $m^{-1}K^{-1}$
Thickness	0.01 m
Area	0.1*0.1 m^2

Table 5-2 **PCM properties**

5.1.4 Results

A validation of the results is performed comparing some results with those obtaining by Zhu et al.[47]

The temperature fluctuation across the thermoelectric device is presented in the Fig below.

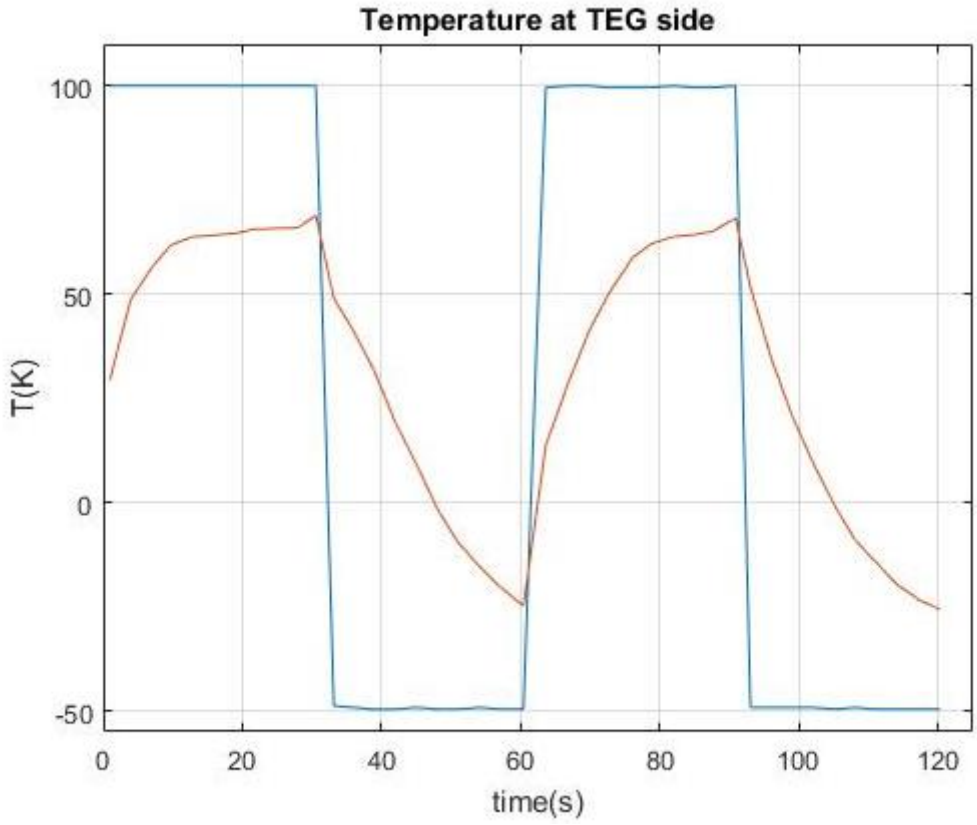

Figure 5-1 Temperature evolution at TEG sides. The external temperature profile is the blu one and the temperature in the thermoelectric device is the red one.

The actual temperature gradient is much lower than the one computed, no contact resistance has been considered.

As illustrated in the figure above, external temperature profile of TEG (blue curve) varies according to the ambient temperature, which can be divided into two sections - heating state (0–30 min) and cooling state (30 –60 min). As the heating phase starts, The temperature in the thermoelectric device (red curve) rises rapidly and then the growth becomes slow as the temperature exceeds 60 °C due to thermal storage via phase change process. As the thermal conductivity of the PCM increases the temperature difference decreases. In particular in the absence of the PCM the temperature difference is just 13°C, in the case considered it can achieve 30°C of course increasing the energy gained. As the ambient temperature fluctuates, heat flows through the TEG, and the internal temperature follows the external input with a delay that depends on the property of PCM. However, it is certain that the latent heat of PCM gets reduced as the percent content of the thermal conductivity enhancer is increased. Of course, the melting temperature of the PCM plays an important role in the analysis.

The open circuit voltage and the output power per unit volume are obtained.

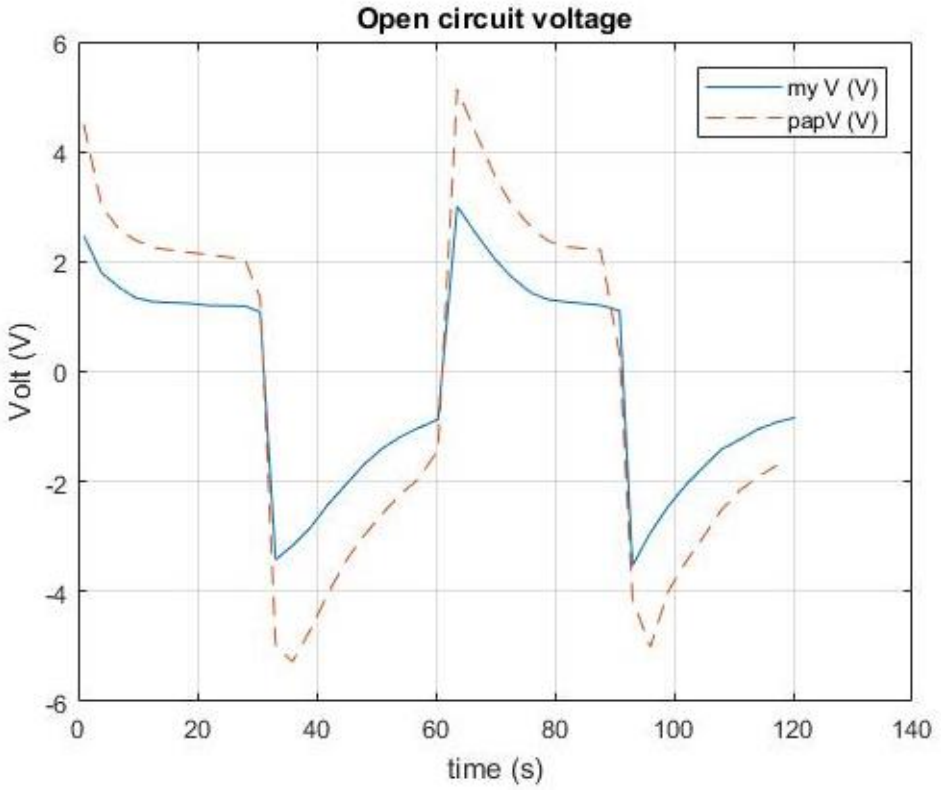

Figure 5-2 Open circuit voltage. The computed profile (blue curve) is compared with the profile obtained in literature (dotted curve).

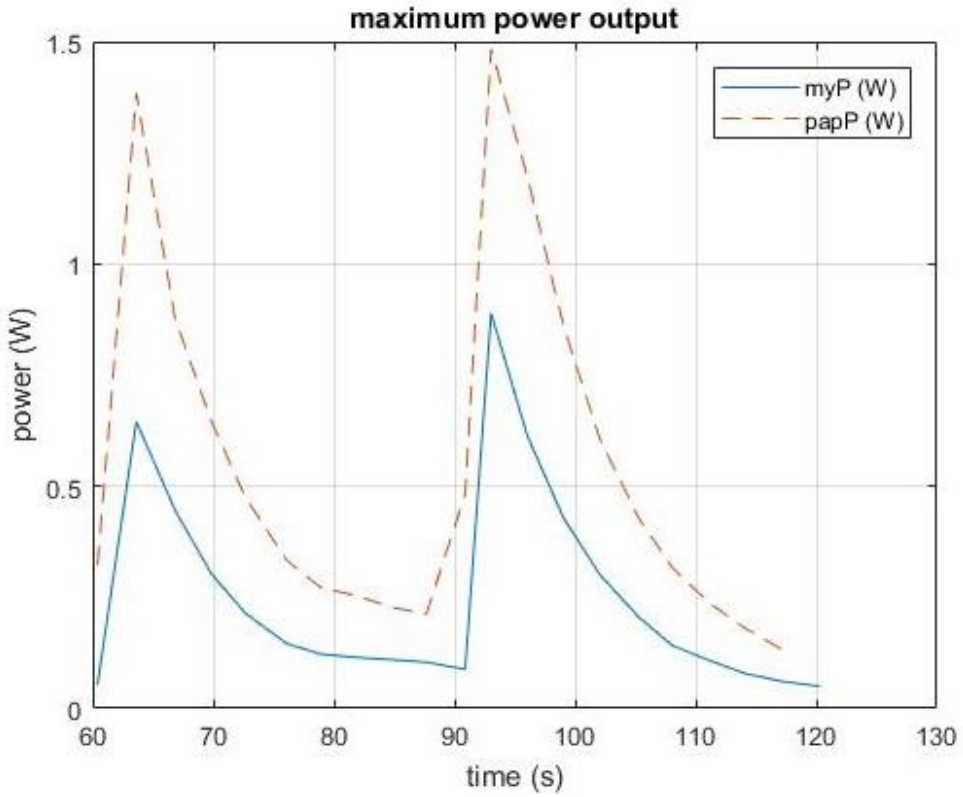

Figure 5-3 Maximum power output. The computed power (blue curve) is compared with the one obtained in literature (dotted curve).

Using equation of $E = \int_0^t P\ dt$ the total electrical energy (E) can be easily obtained. In particular, 2227J are obtained for this analysis. PCM characteristics and suitable melting temperature can enhance the energy output of the system. This is just one of the possibilities of employ a PCM for a power generation. In this case we have seen how the presence of a phase change material can affect the temperature difference across a thermoelectric material with an increase of performances. Another possibility could be a coupling between a PCM and a pyroelectric material.

5.2 Pyroelectric energy harvesting

To harvest waste heat thermoelectric materials have attracted interest, with a number of commercial supplies of thermo-electric generators (TEGs). Thermoelectric materials and systems generate electrical power from temperature gradients (dT/dx) while pyroelectric materials produce power from temperature fluctuations (dT/dt) and have some similarities to the way in which piezoelectric harvesters convert mechanical oscillations (ds/dt) into electricity.

Pyroelectric energy conversion is a novel energy process which directly transforms waste heat energy from cyclic heating into electricity via the pyroelectric effect. Application of a periodic temperature profile to pyroelectric cells is necessary to achieve temperature variation rates for generating an electrical output[51].

Pyroelectric materials have the potential to operate with high thermodynamic efficiency and, compared to thermoelectric generators, do not require bulky heat sinks to maintain the temperature gradient. Pyroelectric materials respond to changes in temperature which cause an internal strain, and this, in turn, results in electrical charges on the material's surface.

All pyroelectrics are polar materials and exhibit a spontaneous polarization Ps in the absence of an applied electric field. The presence of a spontaneous polarization in the material leads to the presence of a charge on each surface of the material and free charges, such as ions or electrons, are attracted to the charged surfaces of the material. The polarization level is dependent on material temperature.[52] When it is heated there is a decrease in its level of spontaneous polarization as dipoles within the material lose their orientation due to thermal vibrations. This fall in the polarization level leads to a decrease in the number of free charges bound to the material surface. If the material is under open circuit conditions the free charges remain at the electrode surface and an electric potential is generated across the material. If the material in under short circuit conditions an electric current flows between the two polar surfaces of the material[52].

To maximize the pyroelectric current under short circuit conditions, the pyroelectric should have a large surface area, large pyroelectric coefficient and a high rate of temperature change.

$$i = pA\frac{dT}{dt}$$

Where p is the pyroelectric coefficient given by the:

$$p = \frac{dPs}{dT}$$

Ps represents the spontaneous polarization of the material. Pyroelectric coefficients are strongly dependent on the layer structure and processing[53].

To maximize the pyroelectric current under short-circuit conditions, clearly the pyroelectric should have a large surface area, large pyroelectric coefficient and a high rate of temperature change. The equation implies that the generated current is independent of thickness and proportional to area since the current is simply associated with the surface charge.

5.2.1 Pyroelectric materials

Nowadays, commercial pyroelectric sensors are already popular for industrial and everyday applications. In most cases the largest pyroelectric effects are observed in a class of materials known as ferroelectrics. Examples of ferroelectrics single crystals used in pyroelectric devices include triglycine sulphate (TGS) (NH2CH2COOH)3H2S, lithium tantalate and the tungsten bronze strontium barium niobate.

TGS and the family of isomorphous compounds have provided some of the highest pyroelectric figures of merit. TGS possesses a Curie temperature of 49°C [54] below which is polar. Although it provides the highest voltage responses, there is a difficulty associated with its water solubility, hygroscopic nature and fragility.

Poyvinylidene fluoride (PVDF) has received much more attention in the last years.[55] The reported pyroelectric coefficients are smaller comparison to TGS family; its polar properties start to degrade if heated much above 80°C. The major advantages which PVDF presents for pyroelectric detectors are that large-area thin films are readily available commercially at low cost.

For high temperature applications one of the possible choices is Lithium tantalate (LiTaO3) which transforms in a non-polar paraelectric at 665°C. It possesses a moderate pyroelectric effect and dielectric constant which combine to give a response figure about one quarter of TGS[54]. However, very low values of dielectric loss have been reported for this material.

Strontium barium niobate is a tungsten bronze ferroelectric with a Curie temperature variable between 195°C and 53°C. It is characterized by a high pyroelectric coefficient, high dielectric constant and low dielectric loss.

Another interesting ferroelectric is PbTiO3 with a high Curie point (490°C). It also possesses a high spontaneous polarization (up to 75 µC cm-2)[54].

5.2.2 Description of the device

We consider a single disk-shape plate of pyroelectric material. The thickness is assumed to be much smaller than the diameter of the plate. Due to the dimension ratio, we assume a uniform temperature of the element. The pyroelectric layer is sandwiched between two electrodes. The uniformity of the temperature was checked trough a MATLAB model in which, during a transient analysis, the temperature was constant across the thickness of the material.

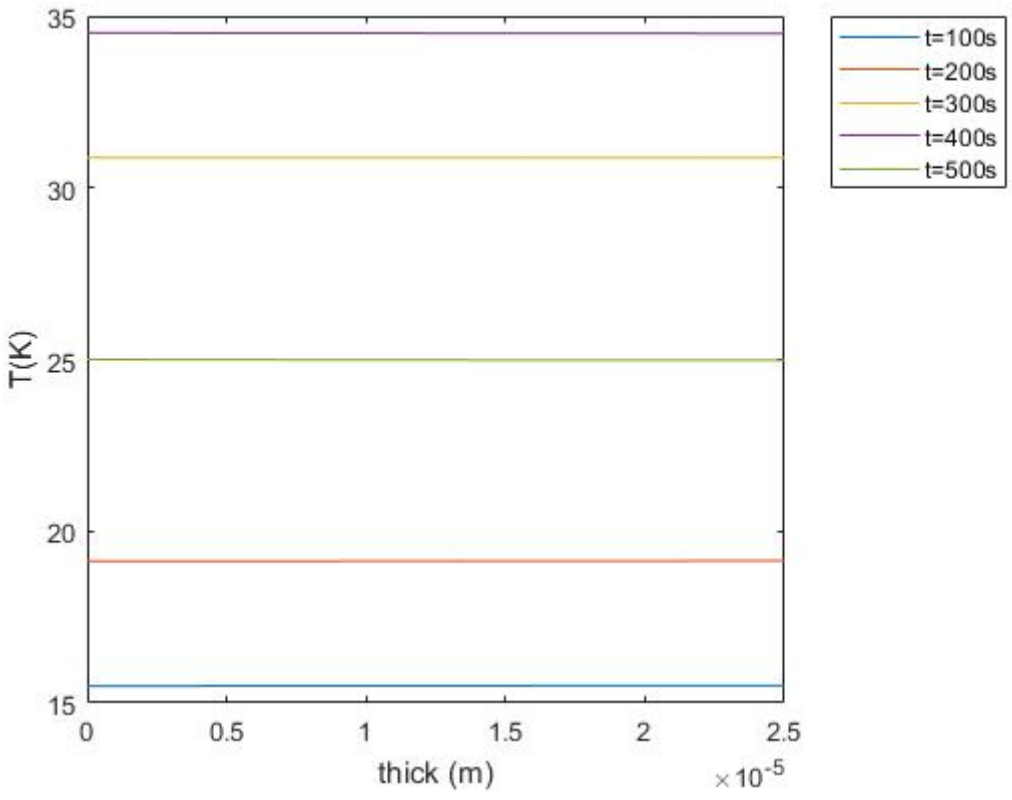

Figure 5-4 Temperature along the thickness of the pyroelectric element at different times. As can be seen it can be considered constant with a good approximation.

5.2.3 Model description

The pyroelectric current is independent of material thickness and only depends on the effective area of the electrode. By integrating current equation with respect to time, the net charge developed due to a temperature change is:

$$Q = p\ A\ \Delta T$$

The relationship between current, pyroelectric coefficient, area and rate of change of temperature can be expressed by the circuit below that includes the pyroelectric current source, the electrical capacitance $\mathrm{C_p}$ and resistance $\mathrm{R_p}$, resulting in an output voltage $\mathrm{V_p}$.

Having converted thermal energy into electrical energy it is necessary to transfer the electrical energy to an external load (e.g. resistor) or storage medium (e.g. capacitor) using a suitable interface[52].

A lumped-parameter model of a pyroelectric element is shown. The pyroelectric element is modelled as a current source in parallel with an internal capacitance. The figure also shows the pyroelectric element connected to an external capacitor and resistor. The objective is to determine the element's output voltage and power generated for a given temperature profile.

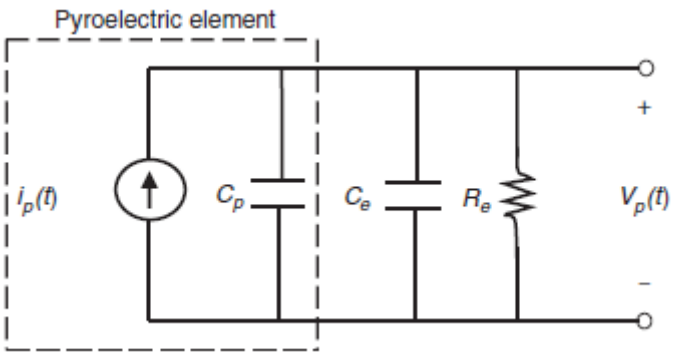

Figure 5-5 A lumped-parameter model of a pyroelectric element, which is modelled as a current source in parallel with an internal capacitance connected in parallel with an external capacitor and resistor. The current is proportional to the rate of change of temperature of the device. The Voltage generated by the pyroelectric element is denoted by $V_p(t)$.

For a given temperature profile, the instantaneous power dissipated by the resistor can be determined as:

$$P(t) = \frac{V_p^2(t)}{R_e}$$

The evaluation of the voltage is described by the equation:

$$C\frac{dV(t)}{dt}+\frac{V(t)}{R}=i_p(t)$$

Where C is the equivalent capacitance for parallel connected pyroelectric capacitance and external capacitor; R is the equivalent resistance for parallel connected leakage resistance of pyroelectric detector and external resistance. As an example, the external capacitance and resistance were chosen as C_e=0 and R_e=1MΩ, respectively. The chosen resistor value was not optimized for maximum power generation.

The model has been validated through a comparison with Xie et al.[56] The temperature evolution in time that is responsible of the current generation is:

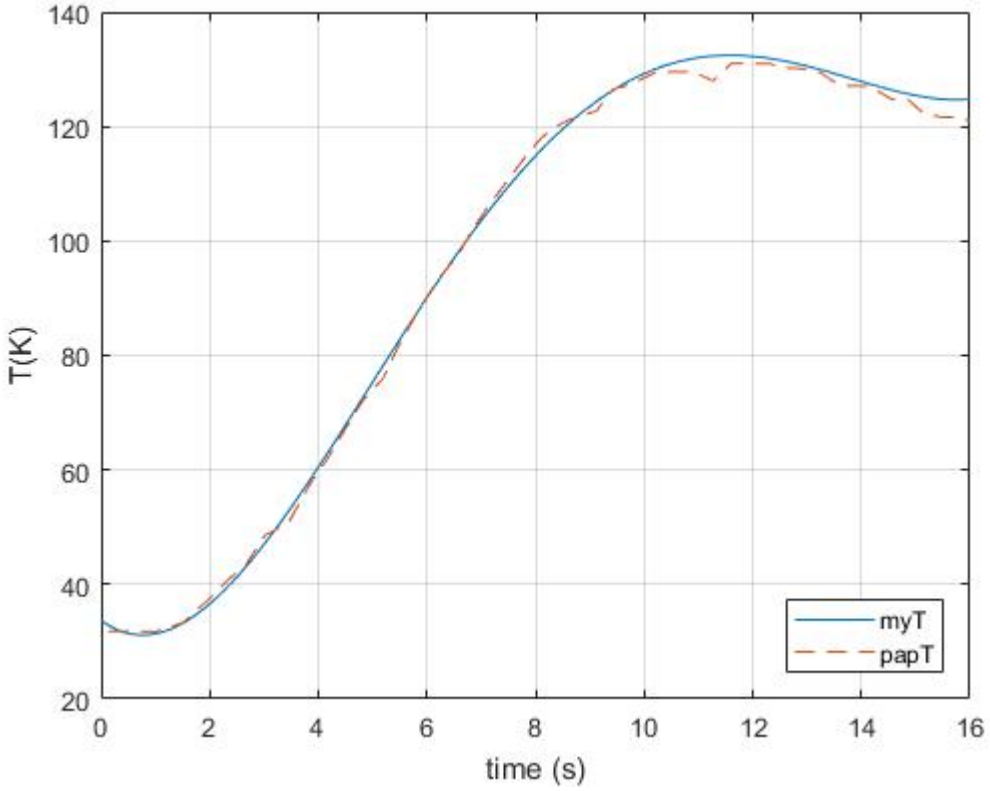

Figure 5-6 Temperature evolution of the pyroelectric element. The computed curve (blue one) is compared with the one obtained in literature (dotted curve).

The voltage across the external resistance and the power dissipated were evaluated.

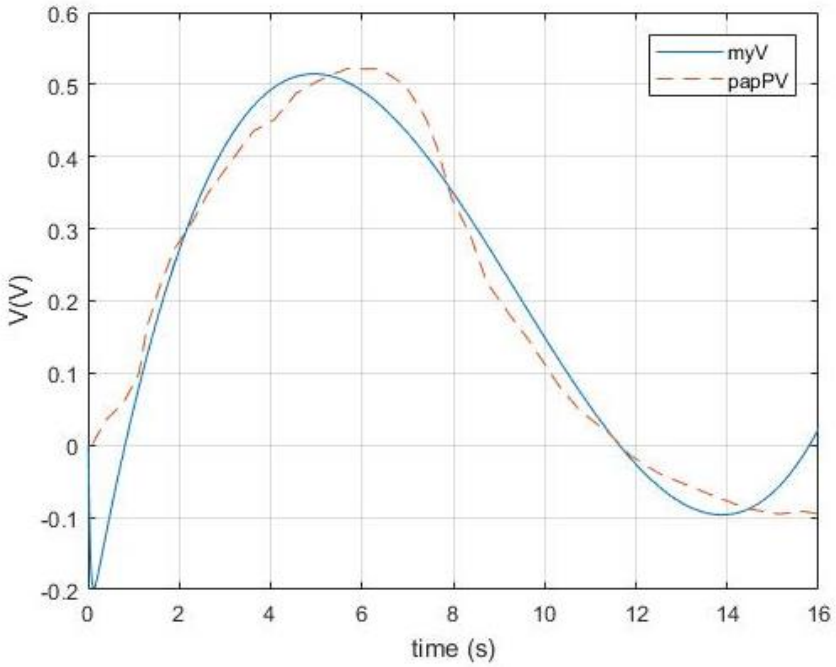

Figure 5-7 Voltage acrossthe external resistance compared with the one resulting from the model of Xie et al.

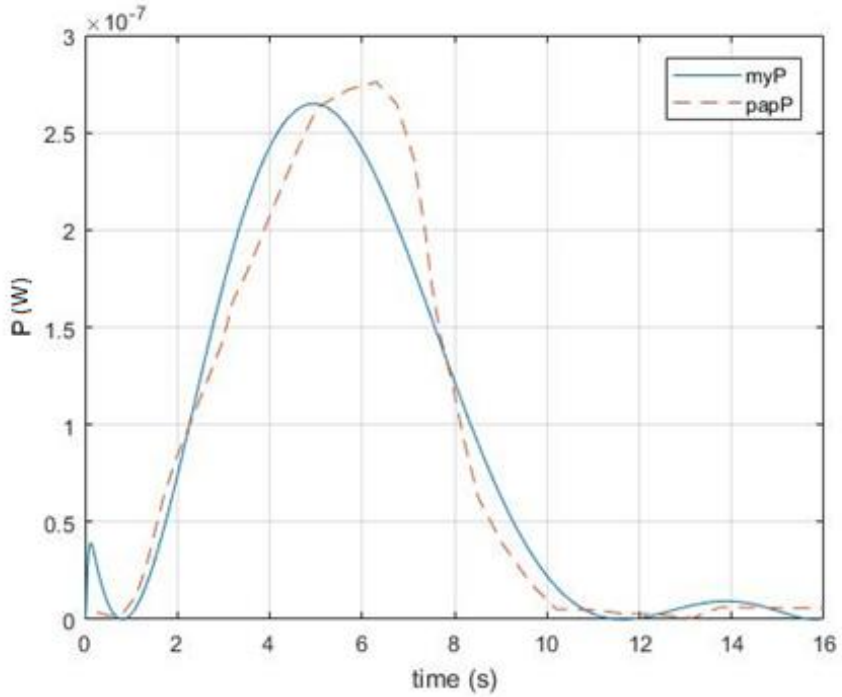

Figure 5-8 Power dissipated in the external resistance. The computed curve (blue one) is compared with the one obtained in literature (dotted curve).

As shown in the figures above, a steep temperature variation lead to a huge power production, so an important requisite is to have not only a temperature variation in time but also a large time derivative to appreciate the voltage generated by the element. The surface area of the element is also an important parameter.

The pyroelectric element used is PZT-5A.

Parameter	Value
Pyroelectric coefficient p	238 µC m^{-2} K^{-1}
Curie Temperature	350 °C
Area	1.44 cm^2
Equivalent capacity Cp	45 nF
Thickness	150 µm

Table 5-3 Pyroelectric material properties

It is important to note that there could be discrepancies in the results attributed to several factors. The temperature of the element has been considered uniform as a good approximation, and it is not perfectly the same, for example at the beginning the is no decrease in temperature in Xie experiment counter our model.

Table 5-4 Comparison of the peak value of voltage and power

Parameter	Modeled	Measured[56]	Difference
Peak voltage (V)	0.51	0.58	12%
Peak power (µW)	0.26	0.33	21%

Apart from the evaluation of the power dissipated in an external resistance, the charge generated from thermal oscillations can be stored in a load capacitor CL using the full-wave rectifier circuit depicted in the figure below.

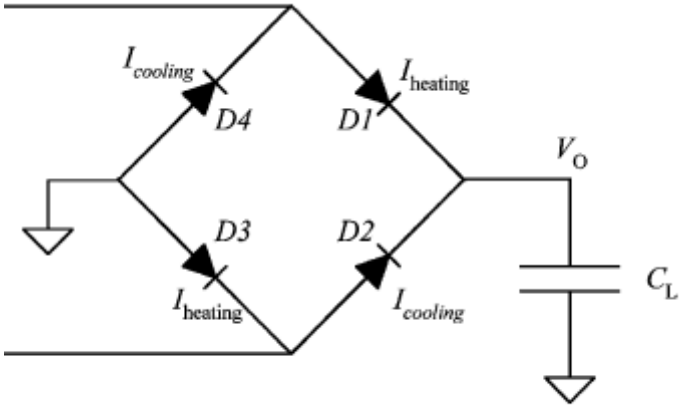

Figure 5-9 Full-wave rectifier circuit used to store the charge provided by a pyroelectric cell

Since pyroelectric devices are bidirectional an alternating thermal drive generates an alternating current and rectification is necessary to harvest the energy.

A typical arrangement is represented by a diode bridge providing full-wave rectification of the output voltage from the device. The harvested energy is stored on the capacitor C_l (1µF); after that can be transferred to the load during time intervals of relatively short duration[57].

During the heating cycle two forward-biased diodes (D1 and D3) let the generated current Ip flow through and charge C_l. The remaining two diodes (D2 and D4) are reversed-biased and block the current flow. During the cooling cycle the direction of I_p is reversed and C_l is charged through D2 and D4. Then, the voltage V_0 across C_l and then the stored energy will increase[53].

When the material is under open circuit conditions, the resulting potential difference, ΔV , across the surface electrodes can be measured[55]:

$$\Delta V = \frac{p}{\varepsilon_0 \varepsilon_{33}^{\sigma}} z\, \Delta T$$

where $\varepsilon_{33}^{\sigma}$ is the dielectric constant of the pyroelectric generator.

Cuadras et al[53] derived V_0 as:

$$V_0(N) = \frac{Q - Qleak - 4\,Vd\,Cp}{2\,Cp}\left[1 - \left(\frac{C_l - Cp}{C_l + Cp}\right)^N\right]$$

Where Vd is the voltage drop across the diodes; Cp is the electrical capacitance of the pyroelectric cell and N is the heating/cooling cycle.

When N tends to infinity, considering the voltage drop of the diode of 0.62V, no leakage and assuming C_1 >Cp:

$$V0, max = \frac{Q - 2.48\ Cp}{2\ Cp}$$

The maximum total energy per unit volume stored by the pyroelectric cell can be expressed[55]:

$$Ec = \frac{1}{2 * vol}\ C\ V^2$$

The critical consideration in a periodic temperature profile for optimizing the pyroelectric harvesters is the frequency or work cycle.

5.2.4 Material selection

In general, we would like the material to have a high pyroelectric coefficient and a low dielectric constant. Relative dielectric constant and pyroelectric coefficient vary with temperature, in this case are considered constant with temperature for simplification.

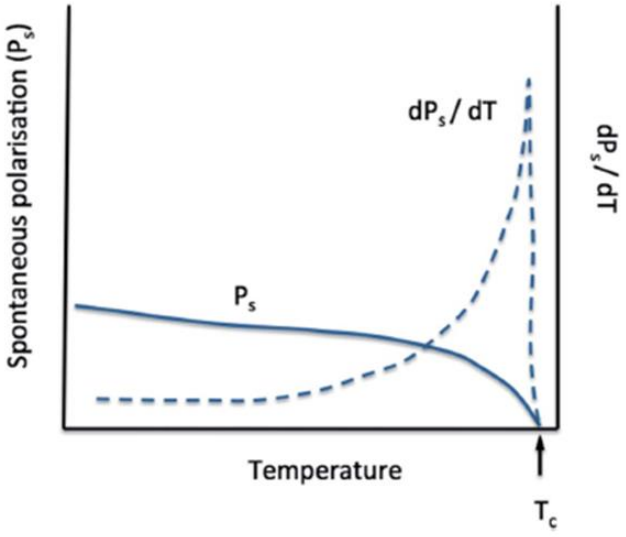

Figure 5-10 Temperature dependence of spontaneous polarisation Ps and pyroelectric coefficient dPs/dT of a ferroelectric material[52]

A variety of figures of merit have been derived for materials selection based on consideration of the thermal and electrical circuits employed. In energy harvesting applications the generated energy or power is a key criterion as well as the overall efficiency of the conversion of the thermal energy to electrical energy.

$$Fe = \frac{p^2}{\varepsilon}$$

where ε is the permittivity in the polarization direction at constant stress.

This figure of merit does not take into account the transient nature of the heat transfer and dielectric losses. An alternative can be:

$$Fe' = \frac{p^2}{\varepsilon\, ce^2}$$

.

Where ce is the volume specific heat (J $m^{-3}\, K^{-1}$) .

The choice of the material for a pyroelectric detector is not as straightforward as might be implied from the values of their figures of merit. Other factors such as environmental stability, availability, cost and manufacturing considerations are also very important and may militate against the use of one material or another. In our case (in the absence of an external electric field able to repolarize the material), there is the necessity to choose a pyroelectric material whose Curie Temperature is higher than the operating temperature. As an example, with an operating temperature of 800°C only LiNO3 is suitable for our application.

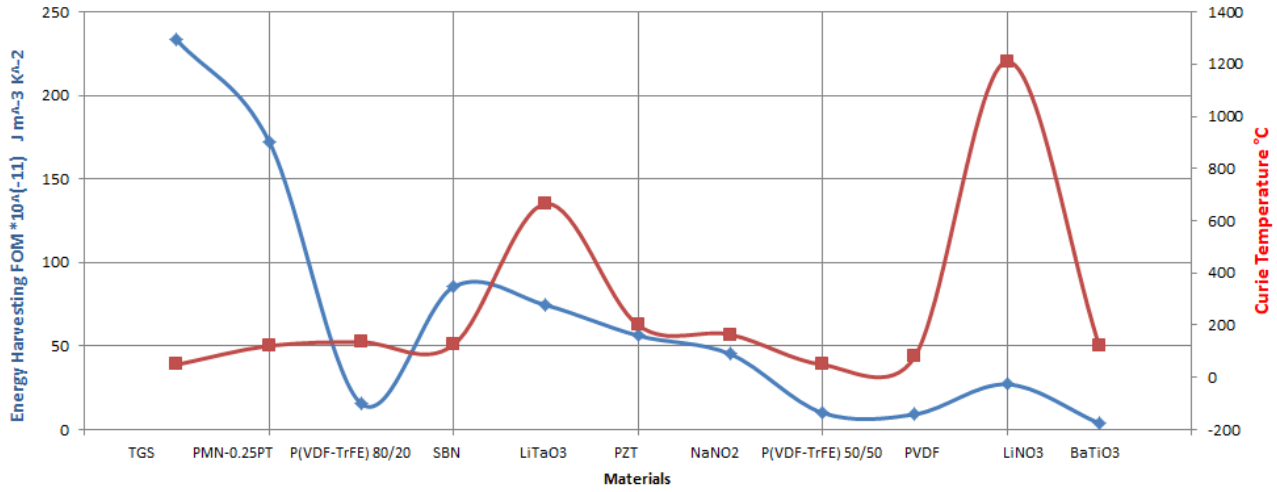

Figure 5-11 Depending on theapplication and the consequent operationg temperature, the choice of the pyroelctric material can be done in different ways.

5.2.5 Results

Another validation is performed evaluating the voltage generated by a pyroelectric material and it is compared with the one evaluated by Odon et al.[58]

Figure below shows the values of current I and temperature T over time. Positive and negative values of I indicate the current flow direction through the sample. I and dT/dt show a similar profile when heating the sample.

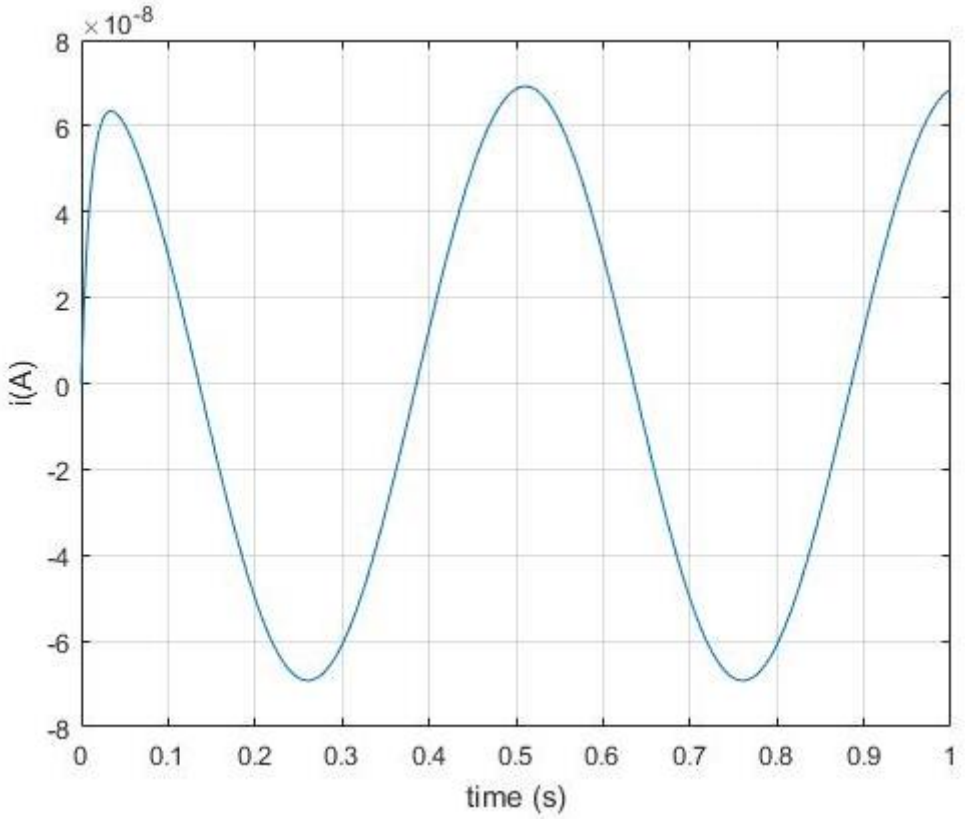

Figure 5-12 **Current generated**

The voltage across the device V has been plotted as a function of time.

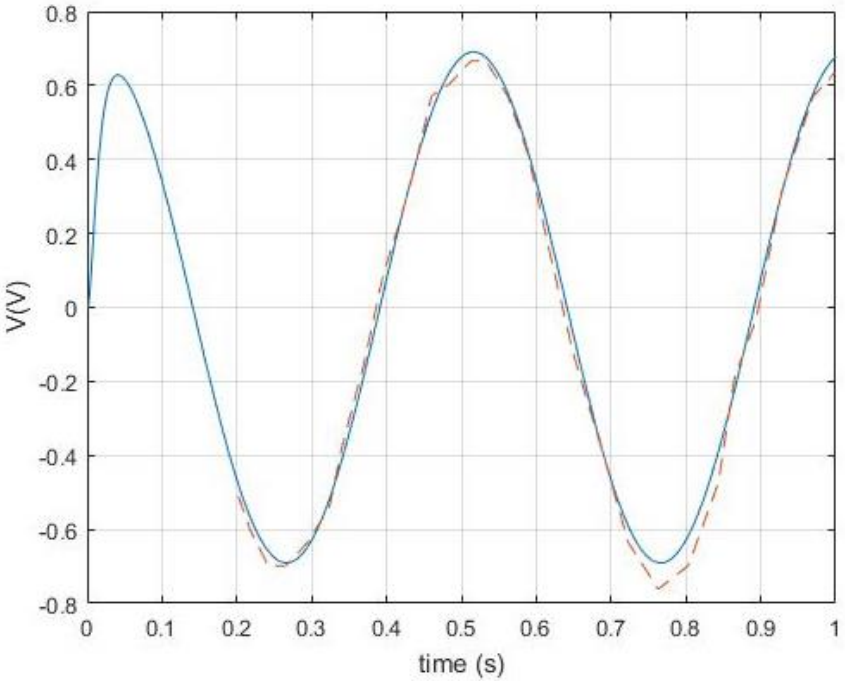

Figure 5-13 Voltage function of time. The computed curve (blue one) is compared with the one obtained in literature (dotted curve).

The stored energy is given by:

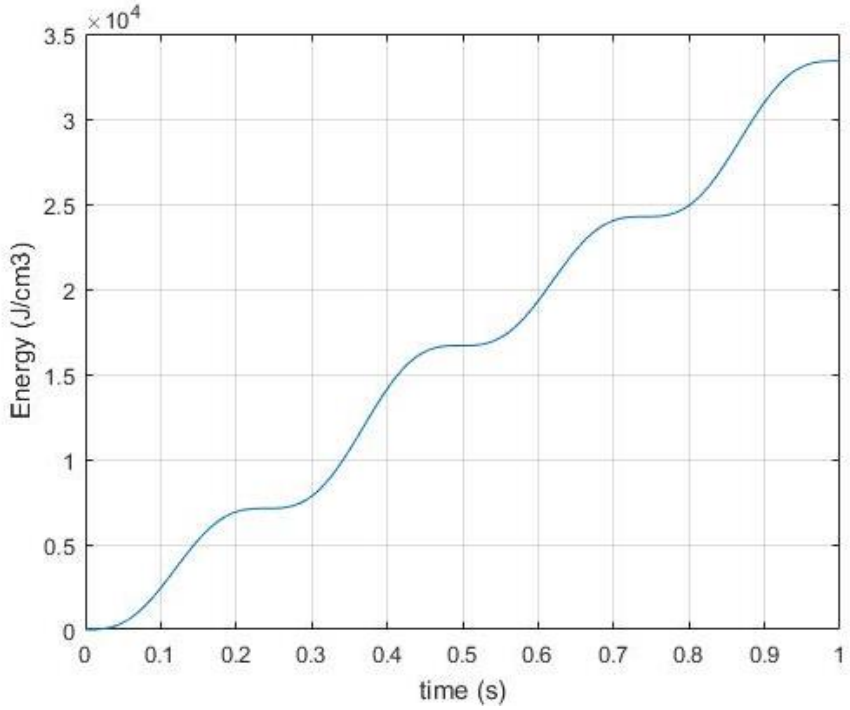

Figure 5-14 Energy stored in an external capacitor

The energy stored in an external capacitor has been evaluated as:

$$E = \frac{1}{2} C V^2$$

It depends on C so large values of C permit to store more energy. However lower values of C lead to a faster increase of V0 and E.

In the case study considered, there is a waste temperature profile with constant values for a certain period. In order to turn this evolution in a continuous time evolution of temperature, a phase change material has been coupled with the pyroelectric material.

The pyroelectric element is PVDF.

Parameter[48]	**Value**
Pyroelectric coefficient $\boldsymbol{p}$	30 C $cm^{-2}\ K^{-1}$
Dielectric permittivity ε	106*10^{-14} F cm^{-1}
Heat capacity C	2.4 J $cm^{-3}K^{-1}$
Area	132*$10^{-2}cm^{-2}$
Equivalent capacity Cp	560 pF
Thickness	25 µm

Table 5-5 Pyroelectric material properties

Cu/G/OD is a kind of suitable phase change material in low temperature applications due to the phase change temperature (about 27°C) and high latent heat of fusion. It was prepared by Cottrill et al.[59] growing multilayer graphene on Cu foams, which is then vacuum impregnated with molten OD.

Items[59]	Value
Material	Cu/G/OD
Density	1300 kg m^{-3}
Latent heat	131000 J kg^{-1}
Phase change	26.9-28.9 °C
temperature	2500 J $kg^{-1}K^{-1}$
Specific heat	10.35 W $m^{-1}K^{-1}$
Thermal conductivity	0.013 m
Thickness	0.015^2 m^2
Area	

Table 5-6 PCM properties

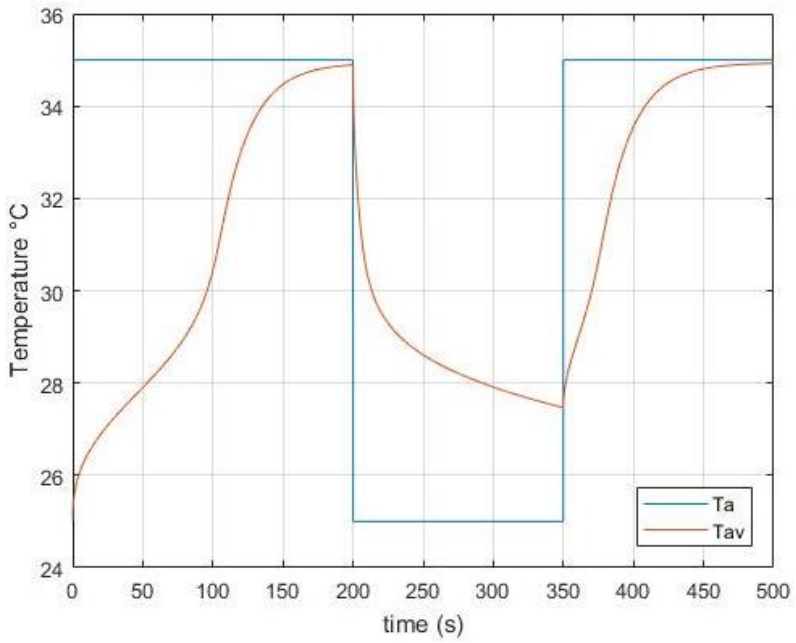

Figure 5-15 Temperature evolution with and without PCM. The ambient temperature (blue curve) has a step evolution in time, the average temperature of the PCM (red curve) follows the ambient variation.

Thanks to the PCM the new temperature profile is not flat anymore, so there is the possibility to exploit this evolution. The current and the resulting voltage across the pyroelectric material are presented for materials with different properties coupled with our pyroelectric element. This was performed in order to understand a link between the power production and different materials properties.

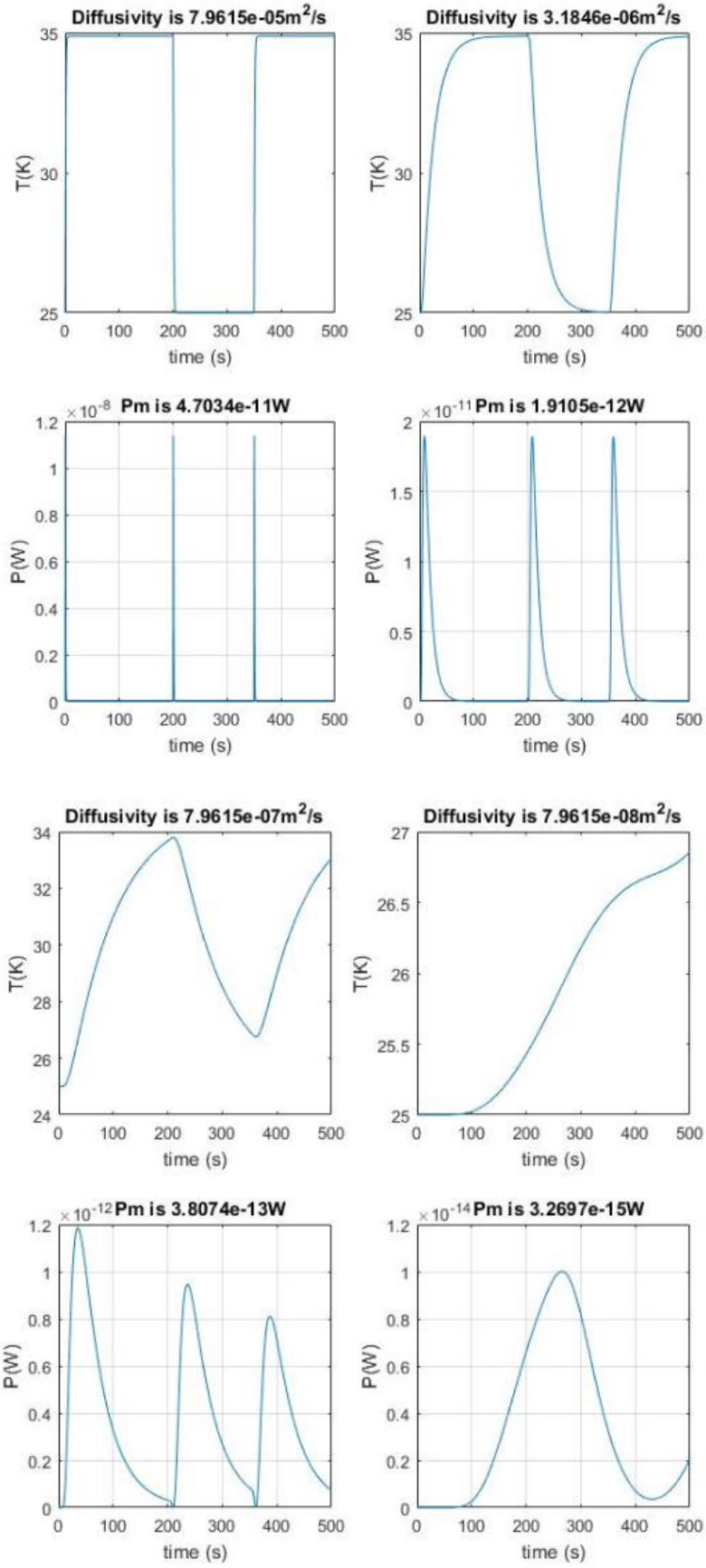

Figure 5-16 Temperature evolution and dissipated power for different materials with different diffusivities.

With a higher diffusivity the power production is higher this is due to the faster response of the material to the external change in temperature but we can see that the power production is limited to abrupted change in temperature. With a lower diffusivity we can obtain a less production but more stable. The impulsive production can cause damages to elements of the circuit. In addiction to this, the time for which the power is different from zero is higher with the presence of a phase change material.

The same analysis was done in order to obtain different diffusivity changing the thermal conductivity, density or specific heat capacity.

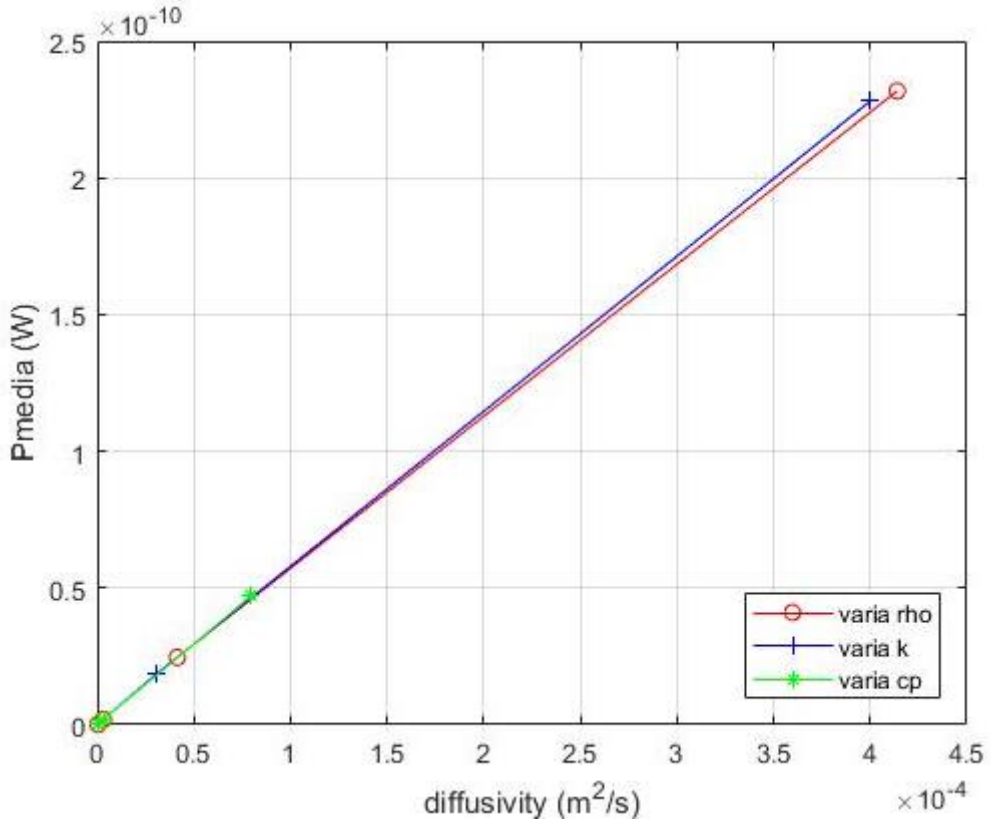

Figure 5-17 Variation of the average of the dissipated power in the external resistance in function of the diffusivity of the material.

As we can see improving the thermal conductivity it is possible to obtain a higher power production.

5.3 Comparison

Thermoelectric energy harvesting requires ensuring the maximum temperature gradient between the hot and cold surface, and this capability depends on the surface heat exchange and heat conductivity. Materials exhibiting a large ZT value usually also exhibit quite large heat conductivities; consequently, for large temperature gradient a huge surface heat exchange is required. On the contrary, pyroelectric energy harvesting is optimal when the temperature period is larger than the time constant defined as[48]

$$\tau = \frac{e\ c}{h}$$

where e, c and h are the thickness heat capacity and surface heat exchange respectively.

So that for the pyroelectric case we face an optimization of periodic heat transfer whereas in the thermoelectric case, we face the optimization of the heat flow.

Although pyroelectric energy harvesting may seem to give little energy, it has a greater efficiency compared to the thermoelectric case and it is much easier to get it to work using limited surface heat exchanges.

6. Conclusions

The present work dealt with the selection, model formulation, fabrication and testing of a novel composition of a Shape Stabilized Phase-Change material (SSPCM) for Latent Heat Thermal Energy Storage purpose.

The main focus of the experimental analysis was primarily devoted to address the form-stability concept linked to a multi-component composite. The high-thermal capacity of the supporting material (Vermiculite) and the enhanced thermal conductivity of the added Graphite made the studied formulation a valid option for waste heat recovery for medium-to-high melting temperature. Furthermore, this configuration allows to exploit heat in a wider range of operating temperatures (from ambient to 220-250°C) when the fraction of sensible heat is accessed.

The composites were fabricated following the mixing, cold-compression and sintering method and they achieved a good shape stability even with a diameter of 50mm. The micro-structural analysis and the thermo-physical properties investigation provided fundamental tools to shed a light onto the novel-manufactured SSPCMs contributing to demonstrate the high-reproducibility, controllability of fabricating parameters and cost-effectiveness of the specific manufacturing procedure. In fact, an important achievement would be the possibility of a mass production of this type of composites that is now limited to lab analysis.

The experimental analysis highlighted that form-stability and heat transfer enhancement of the manufactured pellets is strictly connected to the typology of materials involved and to the chosen manufacturing process and the variable parameters connected with it. Dealing with enhanced graphitic formulations, the introduction of graphite in several forms through the adoption of cold/warm compression techniques after mixing in powder form, determined higher heat enhancement compared to some infiltration and dispersion techniques. Shape-stability is the outcome of complementary effects when dealing with porous materials constituting a highly porous matrix, which accounts both for the effect of capillarity forces counterbalanced by interfacial tensions but also because of fluid-mechanical issues. For some materials, a minimum porosity must be created to accommodate volume expansion meanwhile maintaining the structural integrity of the PCM.

Through the use of the X-ray tomography, a correlation between the porosity and the thermal conductivity was highlighted. In particular, a vermiculite particles size of 1 mm is eligible for the creation of a network inside the composite that can enhance thermal conduction. A different contribution of open and closed porosity is given to the formation of thermal conduction network.

The importance of PCM materials is not only related to sensible heat storage but also to power production. In many applications there is a large amount of waste heat that presents different evolution in time. This amount of heat can be stored or used for electrical energy

generation in thermoelectric and pyroelectric devices. A phase change material coupled with these devices can optimize the power production if its properties are correctly matched. Two examples of this application were analysed: Thermoelectric Generators (TEGs) and pyroelectric devices.

Combining the PCM with TEGs exhibits great advantage of continuous power production maximizing the temperature difference. Furthermore, a good PCM should possess the characteristics of high heat fusion per unit mass, proper melting temperature, high thermal conductivity, thermal stability, non-toxicity and non-corrosiveness.

As far as the combination of the PCM and a pyroelectric device for power production is concerned, an example of step temperature trend was considered. The presence of the phase change material gives the possibility to have a temperature evolution in time even in the case of a constant external source avoiding abrupt temperature variation that can lead to the damage of auxiliary components in the circuit. As a case study, a disk of pyroelectric material in contact with a PCM was analyzed. The resulting model, validated through literature, showed that the most important characteristic for enhancing power generation is the diffusivity of the PCM considered. The optimal enhancement of the thermal diffusivity was determined by the improvement of the thermal conductivity through the use of a thermal enhancer such as the graphite powder used in the fabrication procedure of this work. In conclusion, considering the importance of high thermal conductivity in PCMs, this work highlighted the relationship between the manufacturing process, porosity and thermal conductivity trying to understand how the particles size can affect the porosity and the micro-structure of the composite.

Cost-effective manufacturing processes and materials along with the PCM characteristics needed for the fabrication of devices for power production exploiting waste heat sources, confirm the great future potential of such technologies.

Bibliography

1. Phys JA. Pyroelectric waste heat energy harvesting using the Olsen cycle on Pb (Zr , Ti) O3-Pb (Ni , Nb) O3 ceramics. 2018;174104(November). doi:10.1063/1.5037112

2. Sarbu I. A Comprehensive Review of Thermal Energy Storage. 2018. doi:10.3390/su10010191

3. El-Dessouky H, Al-Juwayhel F. Effectiveness of a thermal energy storage system using phase-change materials. *Energy Convers Manag*. 1997;38(6):601-617. doi:10.1016/S0196-8904(96)00072-6

4. Pielichowska K, Pielichowski K. Phase change materials for thermal energy storage. *Prog Mater Sci*. 2014;65:67-123. doi:10.1016/j.pmatsci.2014.03.005

5. Cabeza LF, Barreneche C, Martorell I, et al. Unconventional experimental technologies available for phase change materials (PCM) characterization. Part 1. Thermophysical properties. *Renew Sustain Energy Rev*. 2015;43:1399-1414. doi:10.1016/j.rser.2014.07.191

6. Solcà N, Dopfer O. Infrared spectra of the phenol-Ar and phenol-N2cations: Proton-bound versus π -bound structures. *Chem Phys Lett*. 2000;325(4):354-359. doi:10.1016/j.solmat.2017.09.046

7. Souayfane F, Fardoun F, Biwole PH. Phase change materials (PCM) for cooling applications in buildings: A review. *Energy Build*. 2016;129:396-431. doi:10.1016/j.enbuild.2016.04.006

8. Zhang P, Xiao X, Ma ZW. A review of the composite phase change materials: Fabrication, characterization, mathematical modeling and application to performance enhancement. *Appl Energy*. 2016;165:472-510. doi:10.1016/j.apenergy.2015.12.043

9. M.N.A. Hawlader, M.S: Uddin M. K. Microencapsulated PCM thermal-energy storage system. *Appl Energy*. 2018;20(5):339. doi:10.3390/e20050339

10. Umair MM, Zhang Y, Iqbal K, Zhang S, Tang B. Novel strategies and supporting materials applied to shape-stabilize organic phase change materials for thermal energy storage–A review. *Appl Energy*. 2019;235(November 2018):846-873. doi:10.1016/j.apenergy.2018.11.017

11. Sari A, Karaipekli A. Thermal conductivity and latent heat thermal energy storage characteristics of paraffin/expanded graphite composite as phase change material. *Appl Therm Eng*. 2007;27(8-9):1271-1277. doi:10.1016/j.applthermaleng.2006.11.004

12. Sari A, Akcay M, Soylak M, Onal A. Polymer-stearic acid blends as form-stable phase change material for thermal energy storage. Journal of Scientific & Industrial Research, 64, 991–996. Retrieved from

http://nopr.niscair.res.in/bitstream. *J Sci Ind Res*. 2005;64(December):991-996. http://nopr.niscair.res.in/bitstream/123456789/5380/1/JSIR 64(12) 991-996.pdf.

13. Fang G, Tang F, Cao L. Preparation, thermal properties and applications of shape-stabilized thermal energy storage materials. *Renew Sustain Energy Rev*. 2014;40:237-259. doi:10.1016/j.rser.2014.07.179

14. Investigation N, Storage TT. Numerical Investigation Investigation of of PCM PCM Melting Melting in in a a Finned Finned Tube Thermal Storage Storage. 2018. doi:10.5772/intechopen.76890

15. Chen P, Gao X, Wang Y, Xu T, Fang Y, Zhang Z. Solar Energy Materials & Solar Cells Metal foam embedded in SEBS / paraf fi n / HDPE form-stable PCMs for thermal energy storage. *Sol Energy Mater Sol Cells*. 2016;149:60-65. doi:10.1016/j.solmat.2015.12.041

16. Chen K, Yu X, Tian C, Wang J. Preparation and characterization of form-stable paraffin/polyurethane composites as phase change materials for thermal energy storage. *Energy Convers Manag*. 2014;77:13-21. doi:10.1016/j.enconman.2013.09.015

17. Wang W, Yang X, Fang Y, Ding J, Yan J. Preparation and thermal properties of polyethylene glycol/expanded graphite blends for energy storage. *Appl Energy*. 2009;86(9):1479-1483. doi:10.1016/j.apenergy.2008.12.004

18. Zhang X, Wen R, Tang C, et al. Thermal conductivity enhancement of polyethylene glycol/expanded perlite with carbon layer for heat storage application. *Energy Build*. 2016;130:113-121. doi:10.1016/j.enbuild.2016.08.049

19. Xie N, Luo J, Li Z, et al. Salt hydrate/expanded vermiculite composite as a form-stable phase change material for building energy storage. *Sol Energy Mater Sol Cells*. 2019;189(September 2018):33-42. doi:10.1016/j.solmat.2018.09.016

20. Jiang Z, Leng G, Ye F, et al. Form-stable LiNO<inf>3</inf>-NaNO<inf>3</inf>-KNO<inf>3</inf>-Ca(NO<inf>3</inf>)<inf>2</inf>/calcium silicate composite phase change material (PCM) for mid-low temperature thermal energy storage. *Energy Convers Manag*. 2015;106(3):165-172. doi:10.1016/j.enconman.2015.09.035

21. Jiang Z, Ouyang T, Yang Y, et al. Thermal conductivity enhancement of phase change materials with form-stable carbon bonded carbon fiber network. *Mater Des*. 2018;143:177-184. doi:10.1016/j.matdes.2018.01.052

22. Min Li, Zhishen Wu JT. Properties of form-stable paraffin/silicon dioxide/expanded graphite phase change composites prepared by sol–gel method. Applied Energy. https://www.infona.pl/resource/bwmeta1.element.elsevier-2b0a11d0-fabb-348b-95cc-fb3c8c931029. Published 2012.

23. Xiao X, Zhang P, Li M. Preparation and thermal characterization of paraffin/metal foam composite phase change material. *Appl Energy*. 2013;112:1357-1366. doi:10.1016/j.apenergy.2013.04.050

24. Warzoha R, Sanusi O, McManus B, Fleischer AS. Evaluation of methods to fully saturate carbon foam with paraffin wax phase change material for energy storage. *Intersoc Conf Therm Thermomechanical Phenom Electron Syst ITHERM*. 2012;(May 2012):834-839. doi:10.1109/ITHERM.2012.6231513

25. Ge Z, Ye F, Cao H, Leng G, Qin Y, Ding Y. Carbonate-salt-based composite materials for medium- and high-temperature thermal energy storage. *Particuology*. 2014;15:77-81. doi:10.1016/j.partic.2013.09.002

26. Lachheb M, Adili A, Albouchi F, Mzali F, Ben Nasrallah S. Thermal properties improvement of Lithium nitrate/Graphite composite phase change materials. *Appl Therm Eng*. 2016;102:922-931. doi:10.1016/j.applthermaleng.2016.03.167

27. Liu J, Wang Q, Ling Z, Fang X, Zhang Z. A novel process for preparing molten salt/expanded graphite composite phase change blocks with good uniformity and small volume expansion. *Sol Energy Mater Sol Cells*. 2017;169(May):280-286. doi:10.1016/j.solmat.2017.05.046

28. Xu Y, He YL, Zhu GH, Lv S, Shan B. Al/Al2O3Form-Stable Phase Change Material for High Temperature Thermal Energy Storage. *Energy Procedia*. 2017;105:4328-4333. doi:10.1016/j.egypro.2017.03.907

29. Qin Y, Yu X, Leng GH, Zhang L, Ding YL. Effect of diatomite content on diatomite matrix based composite phase change thermal storage material. *Mater Res Innov*. 2014;18(sup2):S2-453-S2-456. doi:10.1179/1432891714Z.000000000449

30. Li R, Zhu J, Zhou W, Cheng X, Li Y. Thermal properties of sodium nitrate-expanded vermiculite form-stable composite phase change materials. *JMADE*. 2016;104:190-196. doi:10.1016/j.matdes.2016.05.039

31. Leng G, Qiao G, Xu G, Vidal T, Ding Y. Erythritol-Vermiculite form-stable phase change materials for thermal energy storage. *Energy Procedia*. 2017;142:3363-3368. doi:10.1016/j.egypro.2017.12.471

32. Xu B, Ma H, Lu Z, Li Z. Paraffin / expanded vermiculite composite phase change material as aggregate for developing lightweight thermal energy storage cement-based composites. *Appl Energy*. 2015;160:358-367. doi:10.1016/j.apenergy.2015.09.069

33. Cheng WL, Zhang RM, Xie K, Liu N, Wang J. Heat conduction enhanced shape-stabilized paraffin/HDPE composite PCMs by graphite addition: Preparation and thermal properties. *Sol Energy Mater Sol Cells*. 2010;94(10):1636-1642. doi:10.1016/j.solmat.2010.05.020

34. Ren Y, Xu C, Yuan M, Ye F, Ju X, Du X. Ca(NO3)2-NaNO3/expanded graphite composite as a novel shape-stable phase change material for mid- to high-

temperature thermal energy storage. *Energy Convers Manag*. 2018;163(3):50-58. doi:10.1016/j.enconman.2018.02.057

35. Ge Z, Ye F, Cao H, Leng G, Qin Y, Ding Y. Carbonate-salt-based composite materials for medium- and high-temperature thermal energy storage. *Particuology*. 2014;15:77-81. doi:10.1016/j.partic.2013.09.002

36. Jia S, Zhu Y, Wang Z, Chen L, Fu L. Improvement of Shape Stability and Thermal Properties of PCM Using Polyethylene Glycol (PEG)/ Sisal Fiber Cellulose (SFC)/ Graphene Oxide (GO). 2017;18(6):1171-1179. doi:10.1007/s12221-017-7093-z

37. Serrano-ópez R, Fradera J C-LS. Molten salts database for energy applications.

38. S. Zhang1, 2 XYC, , Y. M. Ma1*, Y. C. Ke1, J. K. Zhang1 FSW. The effects of particle size and content on the thermal conductivity and mechanical properties of Al2O3/high density polyethylene (HDPE) composites.

39. Khan Z, Khan Z, Ghafoor A. A review of performance enhancement of PCM based latent heat storage system within the context of materials, thermal stability and compatibility. *Energy Convers Manag*. 2016;115:132-158. doi:10.1016/j.enconman.2016.02.045

40. Version A. The user ' s guide. :1-139.

41. Huang X, Chen X, Li A, et al. Shape-stabilized phase change materials based on porous supports for thermal energy storage applications. *Chem Eng J*. 2018;356(June 2018):641-661. doi:10.1016/j.cej.2018.09.013

42. Alawadhi EM. Thermal analysis of a building brick containing phase change material. *Energy Build*. 2008;40(3):351-357. doi:10.1016/j.enbuild.2007.03.001

43. Mirzaei PA, Haghighat F. Modeling of phase change materials for applications in whole building simulation. *Renew Sustain Energy Rev*. 2012;16(7):5355-5362. doi:10.1016/j.rser.2012.04.053

44. Ruciński A, Rusowicz A. Thermoelectric Generation of Current-Theoretical and Experimental Analysis. *Arch Thermodyn*. 2017;38(4):3-13. doi:10.1515/aoter-2017-0021

45. Kiziroglou ME, Wright SW, Toh TT, Mitcheson PD, Becker T, Yeatman EM. Design and fabrication of heat storage thermoelectric harvesting devices. *IEEE Trans Ind Electron*. 2014;61(1):302-309. doi:10.1109/TIE.2013.2257140

46. Zhang X, Zhao LD. Thermoelectric materials: Energy conversion between heat and electricity. *J Mater*. 2015;1(2):92-105. doi:10.1016/j.jmat.2015.01.001

47. Zhu W, Tu Y, Deng Y. Multi-parameter optimization design of thermoelectric harvester based on phase change material for space generation. *Appl Energy*. 2018;228(March):873-880. doi:10.1016/j.apenergy.2018.06.151

48. Sebald G, Guyomar D, Agbossou A. On thermoelectric and pyroelectric energy

harvesting. *Smart Mater Struct*. 2009;18(12). doi:10.1088/0964-1726/18/12/125006

49. RubiTherm GmbH, RT- Data Sheets, Mendeley Data 2011.

50. Gao J, Yan T, Xu T, Ling Z, Wei G, Xu X. Development and experiment validation of variable-resistance-variable-capacitance dynamic simplified thermal models for shape-stabilized phase change material slab. *Appl Therm Eng*. 2019;146(September 2018):364-375. doi:10.1016/j.applthermaleng.2018.09.124

51. Hsiao CC, Jhang JW. Pyroelectric harvesters for generating cyclic energy. *Energies*. 2015;8(5):3489-3502. doi:10.3390/en8053489

52. Bowen CR, Taylor J, Leboulbar E, Zabek D, Chauhan A, Vaish R. Pyroelectric materials and devices for energy harvesting applications. *Energy Environ Sci*. 2014;7(12):3836-3856. doi:10.1039/c4ee01759e

53. Cuadras A, Gasulla M, Ferrari V. Thermal energy harvesting through pyroelectricity. *Sensors Actuators, A Phys*. 2010;158(1):132-139. doi:10.1016/j.sna.2009.12.018

54. Whatmore RW. Pyroelectric devices and materials. *Reports Prog Phys*. 1986;49(12):1335-1386. doi:10.1088/0034-4885/49/12/002

55. Zabek D, Taylor J, Bowen CR. Performance of thin film polyvinylidenefluoride (PVDF) for pyroelectric energy harvesting. *2014 Jt IEEE Int Symp Appl Ferroelectr Int Work Acoust Transduct Mater Devices Work Piezoresponse Force Microsc ISAF/IWATMD/PFM 2014*. 2014:0-3. doi:10.1109/ISAF.2014.6923020

56. Ie JX, Ane XPM, Reen CWG, Ossi KMM, Eang KAMKL. Performance of Thin Piezoelectric Materials for Pyroelectric Energy Harvesting. 2010;21(February). doi:10.1177/1045389X09352818

57. Dalola S, Ferrari V, Marioli D. Pyroelectric effect in PZT thick films for thermal energy harvesting in low-power sensors. *Procedia Eng*. 2010;5:685-688. doi:10.1016/j.proeng.2010.09.202

58. Odon A. Modelling and simulation of the pyroelectric detector using MATLAB/Simulink. *Meas Sci Rev*. 2010;10(6):195-199. doi:10.2478/v10048-010-0033-3

59. Liu P, Cottrill AL, Liu AT, et al. Ultra-high thermal effusivity materials for resonant ambient thermal energy harvesting. *Nat Commun*. 2018;9(1):1-11. doi:10.1038/s41467-018-03029-x